Cite this article as: Park J.-H., et al. (2024). Early-Onset Hearing Loss in Mouse Models of Alzheimer's Disease and Increased DNA Damage in the Cochlea, *AgingBio*, *2*, e20240025. doi: 10.59368/agingbio.20240025.

Research Paper

Early-Onset Hearing Loss in Mouse Models of Alzheimer's Disease and Increased DNA Damage in the Cochlea

Jae-Hyeon Park,[1] Burcin Duan Sahbaz,[1] Komal Pekhale,[1] Xixia Chu,[1] Mustafa N. Okur,[1] Mhamed Grati,[2] Kevin Isgrig,[2] Wade Chien,[2,3] Elena Chrysostomou,[4] Lauren Sullivan,[5] Deborah L. Croteau,[1,6] Uri Manor,[5] and Vilhelm A. Bohr[1,7,*]

[1]DNA repair Section, National Institute on Aging, National Institutes of Health, Baltimore, MD, USA
[2]National Institute on Deafness and Other Communication Disorders, National Institutes of Health, Bethesda, MD, USA
[3]Department of Otolaryngology-Head & Neck Surgery, Johns Hopkins School of Medicine, Baltimore, MD, USA
[4]Waitt Advanced Biophotonics Center, Salk Institute for Biological Studies, La Jolla, CA, USA
[5]Department of Cell & Developmental Biology School of Biological Sciences University of California, San Diego, La Jolla, CA, USA
[6]Computational Biology & Genomics Core, National Institute on Aging, National Institutes of Health, Baltimore, MD, USA
[7]Danish Center for Healthy Aging, University of Copenhagen, Copenhagen N, Denmark
[*]Corresponding author: vbohr@sund.ku.dk
https://doi.org/10.59368/agingbio.20240025

There is considerable interest in whether sensory deficiency is associated with the development of Alzheimer's disease (AD). Notably, the relationship between hearing impairment and AD is of high relevance but still poorly understood. In this study, we found early-onset hearing loss in two AD mouse models, 3xTgAD and 3xTgAD/Polβ$^{+/-}$. The 3xTgAD/Polβ$^{+/-}$ mouse is DNA repair deficient and has more humanized AD features than the 3xTgAD. Both AD mouse models showed increased auditory brainstem response (ABR) thresholds between 16 and 32 kHz at 4 weeks of age, much earlier than any AD cognitive and behavioral changes. The ABR thresholds were significantly higher in 3xTgAD/Polβ$^{+/-}$ mice than in 3xTgAD mice at 16 kHz, and distortion product otoacoustic emission signals were reduced, indicating that DNA damage may be a factor underlying early hearing impairment in AD. Poly ADP-ribosylation and protein expression levels of DNA damage markers increased significantly in the cochlea of the AD mice but not in the adjacent auditory cortex. Phosphoglycerate mutase 2 levels and the number of synaptic ribbons in the presynaptic zones of inner hair cells were decreased in the cochlea of the AD mice. Furthermore, the activity of sirtuin 3 was downregulated in the cochlea of these mice, indicative of impaired mitochondrial function. Taken together, these findings provide new insights into potential mechanisms for hearing dysfunction in AD and suggest that DNA damage in the cochlea might contribute to the development of early hearing loss in AD.

Introduction

Alzheimer's disease (AD) is a progressive neurodegenerative disorder characterized by extensive accumulation of amyloid-β plaques, neurofibrillary tangles consisting of hyperphosphorylated tau protein aggregates, severe neuroinflammation, synaptopathy, and neuronal loss[1,2]. Clinically, AD presents as a syndrome of progressive memory and functional loss through cognitively unimpaired and mild cognitive impairment[3]. Approxiately 5.8 million people in the United States age 65 and older are affected, and the prevalence is projected to increase to 13.8 million by 2050[4]. The identification of AD risk factors helps intercept the disease and slow its progression. Age is the most important risk factor for the development of AD[5]. AD has also been reported to be associated with sensorineural hearing loss[6] in humans, and hearing loss has been proposed to be the largest modifiable risk factor for AD[7].

Hearing loss is the third most common health defect in adults, after heart disease and arthritis, affecting almost half of individuals over the age of 75[8]. Many neurological disorders manifest with hearing loss along with central nervous system symptoms[9]. A growing number of studies in recent years have suggested that older people with hearing loss are more likely to develop AD and dementia, and there has been increasing research interest in the correlation between hearing impairment and cognitive decline[10]. An early study of 156 patients with AD suggested that hearing loss was an early indicator of cognitive dysfunction[11]. It was reported that AD patients may have difficulty with dichotic listening[12–14], understanding speech in the presence of background noise[15,16], impairment of hearing sensitivity[13,17], and impaired sound location[15,18,19]. Studies have addressed the association between hearing impairment and AD; however, hearing measurements in AD individuals are often complicated by a lack of optimal communication with the patient[10,20]. Animal studies provide an invaluable opportunity to investigate the underlying mechanisms of an association between AD and hearing loss. 5xFAD mouse models at 13–14 months of age exhibit

hearing loss at frequencies between 8 and 32 kHz. At 3 months of age, APP/PS1 AD mice had significantly higher auditory brainstem response (ABR) thresholds than wild-type (WT) mice at frequencies between 8 and 40 kHz. These AD mice show elevated ABR thresholds and apparent hair cell loss[21,22]. It has also been reported that the 3xTgAD mouse, which expresses mutant forms of human Aβ precursor protein (APP), presenilin-1 that cause early-onset familial AD, and a tau mutation that causes frontotemporal dementia[23], showed progressively abnormal ABR from 9 months of age[24]. Interestingly, loss of spiral ganglion neurons, but not hair cells, was observed in these 3xTgAD animals[24].

Hair cells are the essential mechanoreceptors in the cochlea converting sound vibrations into electrical signals, which are then transmitted to the brain via the spiral ganglion neurons that innervate the hair cells[25]. Hair cells in the cochlea of humans and other mammals can accumulate damage stemming from a variety of factors, including age, noise, and genetics[26]. Loss of sensory hair cells from the inner ear is the most common cause of sensorineural hearing loss[27–29]. Hair cells are particularly susceptible to oxidative stress-induced death, and mitochondrial oxidative stress is involved in noise-induced hair cell damage and hearing loss[30–32].

Our lab previously created and characterized 3xTgAD/Polβ$^{+/-}$[33]. These mice typically have more progressive AD features relative to the parental 3xTgAD strain[33–35]. Specifically, we have observed greater memory and learning deficits, higher αβ, phosphor-tau levels, and DNA damage marker levels, altered mitophagy, and loss of smelling, another important sensory function[35]. The association of DNA damage with AD is well established. DNA damage accumulation is a risk factor for AD, and much evidence suggests that it may have a causative role in AD progression[36,37]. Excessive oxidative DNA damage, reactive oxygen species production, and mitochondrial dysfunction have been demonstrated in AD, supporting the association with DNA damage and deficient DNA repair. Accumulation of DNA oxidization has been observed in AD patient brains[38,39]. DNA damage was also detected in brains with cognitive impairment[40–42] and preclinical AD. Increased γH2AX, a well-established marker of DNA double-strand breaks, was detected in 11 of 13 AD brains in astrocytes of the hippocampus and cerebral cortex[43]. DNA damage is also implicated in hearing impairment, and DNA damage in the blood is significantly higher in congenital hearing loss patients than in controls[44]. It remains unknown whether DNA damage or repair deficiency is associated with hearing loss in AD. Here, we investigate whether early-onset hearing loss is related to DNA damage and/or repair deficiency in mouse models of AD.

Materials and Methods

Animals

All mouse experiments were performed using protocols approved by the appropriate institutional animal care and use committee of the National Institute on Aging (NIA), Baltimore, in accordance with the national research council's guide for the care and use of laboratory animals. All mice were maintained at a constant temperature with a 12-hour light/dark cycle in the NIA. All mice are on the C57BL/6J background. The breeding methods of Polβ and 3xTgAD/Polβ$^{+/-}$ strains were described previously[33]. Both male and female mice were used in the ABR measurement experiments, with littermate controls used throughout. All experiments were performed blindly using only mouse identification numbers.

ABR recording

Audiometric exam tests were performed in accordance with our previous study protocol[45]. The ABR measurement is a quantitative assessment of the neurological response, measured as evoked potential, detected within 10 ms of an auditory stimulus. ABR audiometry was performed on mice, which were anesthetized via an intraperitoneal injection with a mixture of ketamine (100 mg/kg) and xylazine (10 mg/kg) by use of an MF1 multi-field magnetic speaker in a soundproof chamber. Body temperature was maintained at 36–37 °C by placing anesthetized mice on the deltaphase isothermal pad. Needle electrodes were inserted subdermally (vertex–ventrolateral to pinna). Tone burst stimuli (5 ms duration with a 0.1 ms rise–fall time) were presented at variable volume (10–90 dB SPL) in 5 dB steps at 4, 8, 16, and 32 kHz using an RZ6 system (Tucker Davis Technologies) with Biosig software (Tucker Davis Technologies). For the data analysis, the minimum volume threshold (in dB) that evokes a response at a given frequency was recorded as the outcome measure. n = 7–11 mice per group in males and females.

Distortion product otoacoustic emission (DPOAE) measurement

DPOAE quantifies the electromotility of outer hair cells in the cochlea. DPOAEs were measured by inserting an earplug containing a small microphone (ER-10B+) and two speakers (MF1 multi-field magnetic speaker) in the outer ear canal of each mouse. A series of auditory stimuli were delivered, each composed of two tones at equal decibel level but distinct frequencies, f1 and f2, where $f2 > f1$, $f2/f1 = 1.2$, at $f0 = 10$, 12, 16, and 32 kHz ($f0 = (f1 \times f2)1/2$). The decibel level of both tones varied over the range of 80–10 dB SPL in 5-dB steps. The cubic distortion product at the frequency $2f1 - f2$ was recorded as an average of 512 responses at each frequency tested. DPOAE measurements were made using the RZ6 system (Tucker Davis Technologies) with Biosig software. n = 7–11 mice per group in males and females.

ABR waveform reconstruction

ABR waveform analysis was performed in accordance with our previous study protocol[45]. Raw ABR recording data were extracted using the BioSigRZ software. Voltage values were sampled at a rate of 50,000 Hz (every 0.02 ms) for a duration of 4.5 ms following stimulus presentation. Representative waveforms were calculated and reconstructed offline by averaging the voltage values at each time point using TDT BioSigRZ software. Waves I–V were identified by a series of characteristic peak-to-following-trough forms.

Cochlea dissection and immunofluorescence

Male mice were first subjected to cardiac perfusion using 3% PFA in PBS fixation solution, then decapitated, temporal bones were isolated, and cochlea were directly perfused with 3% PFA through the oval window and incubated for 12 hours in fixative, followed by a decalcification step in 120 mM ethylenediaminetetraacetic acid for 4 days. The organs of Corti from either the left or right ears of WT (n = 5) and 3xTgAD/Polβ$^{+/-}$ mice (n = 5) were microdissected for immunohistochemistry of ribbon synapses. Microdissected cochlea were first permeabilized for 20 min with 0.5% Triton-X100, then blocked overnight with 30% normal goat serum and 3% bovine serum albumin (BSA) in 0.3% Triton-X100 PBS. Primary antibodies diluted 400 times in blocking solution

were incubated for 3 hours at RT rocking. These included mouse anti-CtBP2 (BD Biosciences; Cat# 612044), rabbit anti-Homer1 (Genetex; Cat# GTX103278), guinea pig anti-vGlut3 (Synaptic Systems; Cat# 135204), and chicken anti-neurofilaments (Abcam; Cat# ab134459). Specimens were washed 3 times in 20-min-long PBS baths, and goat secondary antibodies diluted 600 times in blocking solution were applied for 1 hour at RT rocking (ThermoFisher Scientific Cat# A-21124, A-11034, A-21450, and A48260). Specimens were then washed three times in 20-min-long PBS baths and mounted with ProLong Diamond Antifade Mountant (ThermoFisher Scientific; Cat# P36965). Ribbon synapse stacks of super-resolution images were taken using Zeiss AiryScan 880. Decalcified controlateral ears were embedded in paraffin, 5-mm-thick crossections were generated and hematoxylin and eosin-stained, and slides were imaged at Histoserv, Inc. Images were used for a gross examination of diverse cochlea compartments and for counting spiral ganglion neurons.

Hair cell quantification

Two 20× representative regions in each of the turns (apex, middle, and base) of the sensory cochlear epithelium were imaged using an Olympus CKX53 epifluorescence scope. Inner and outer hair cells were manually quantified within two 150 μm representative regions using a Fiji cell counter.

Synapse quantification and analysis

Cytocochleograms were generated by first imaging the individual pieces of dissected cochlear at 4×, then overlaying them with a frequency map using the measure line plug-in tool using Fiji. Confocal z-stacks (110 nm z-step-size) images were obtained using a 100× oil immersion objective on a Zeiss CSU spinning disk microscope at specific frequency regions (4, 16, and 32 kHz). Two images per frequency region were acquired. Max projections of the 3D z-stack images were generated, and regions of interest were drawn around each inner hair cell (IHC). Paired and orphan synapses labeled with pre- and postsynaptic markers, CtBP2 and Homer1, respectively, were manually quantified using the Fiji plug-in cell counter. Synaptic counts were reported as the number of paired/orphan punctae per IHC.

NAD^+ measurement

Mice were anesthetized and dissected with cold PBS buffer, and the cochlea and auditory cortex were weighed and placed in NADH/NAD Extraction Buffer (Abcam, ab65348). Following homogenization with a micropestle, the NAD^+ level was measured with a commercially available NAD^+/NADH assay kit according to the manufacturer's protocol. Two technical replicates were performed on n = 3 mice per condition; NAD^+/NADH levels were normalized to total protein.

Western blot analysis

Male mouse cochlea and auditory cortex tissues in WT (n = 3), Polβ$^{+/-}$ (n = 3), 3xTgAD (n = 3), and 3xTgAD/Polβ$^{+/-}$ (n = 3) mice were homogenized in 1X RIPA lysis buffer (50 mM Tris-HCl, pH 7.4, 150 mM NaCl, 1 mM EDTA, 1 mM EGTA, 1.2% Triton X-100, 0.5% sodium deoxycholate, and 0.1% SDS, Enzo Life Sciences, #ADI-80-1496) containing protease inhibitor cocktail and halt phosphatase inhibitor cocktail (Roche, Indianapolis, IN, USA). The collected samples were sonicated on ice and centrifuged at 10,000 × g for 10 min at 4 °C. The protein concentration was determined with a Bradford reagent. 15 μg proteins were separated on 4%–12% Bis-Tris gel (ThermoFisher Scientific, #NP0336BOX) and transferred to nitrocellulose membranes. Membranes were then blocked for 1 hour at RT in TBS-T (500 mM NaCl, 20 mM Tris, 0.1% Tween 20, pH 7.4) supplemented with 5% nonfat dried milk and BSA. Subsequently, membranes were incubated overnight at 4 °C with primary antibodies, followed by 1 hour at RT with HRP-conjugated secondary antibodies (see **Table S1**, for details of the antibodies used in the study). Proteins were detected using an enhanced chemiluminescent detection system (ECL, EMD Millipore) and the ChemiDoc Imaging System (#12003153) (Bio-Rad Laboratories, USA).

Phosphoglycerate mutase 2 (Pgam2) ELISA measurement

Male mouse Pgam2 was measured using mouse ELISA kits (G-Biosciences, # IT5345, St. Louis, MO, USA) following the manufacturer's protocol. Briefly, the cochlea and auditory cortex tissue (10 mg) in WT (n = 3), Polβ (n = 3), 3xTgAD (n = 3), and 3xTgAD/Polβ$^{+/-}$ (n = 3) mice were homogenized with precooling PBS (pH 7.0–7.2) on ice and centrifuged at 5,000 × g for 5 min at 4 °C. The supernatants were collected and transferred to 96-well plates coated with a specific antibody against the protein of interest, Pgam2. These samples were incubated for a total of 3 hours at 37 °C and washed twice with 350 μL of 1X wash solution to each well using a multichannel pipette for a total of 10 times. ELISA detection substrate (TMB) solution to each well was subsequently added and incubated for 15–20 min at 37 °C after covering with foil. TMB was used to visualize the HRP enzymatic reaction. The enzyme-substrate reaction was terminated by the addition of sulfuric acid (stop solution), and the absorbance value of each well was measured at a wavelength of 450 nm on a microplate ELISA reader (Microplate Manager v5.2.1 software, Bio-Rad Laboratories).

RNA extraction and quantitative real-time PCR (qPCR)

RNA was extracted with a PureLink™ RNA Mini Kit (ThermoFisher Scientific, #12183018A) as per the manufacturer's protocol from mouse cochlea and auditory cortex of brain tissues in WT (n = 3), Polβ (n = 3), 3xTgAD (n = 3), and 3xTgAD/Polβ$^{+/-}$ (n = 3) mice. cDNA was synthesized using the PrimeScript™ RT reagent kit (Takara, #RR037A), and qPCR analysis was done with the power SYBR Green PCR master mix (ThermoFisher, #A46109). The primers used to amplify each transcript were the following: Pgam2 (Forward: 5′-CAA GAG AAC CGT TTC TGT GGC T-3′ and Reverse: 5′-CCC ACA TTT GGT CCG TAA CAT C-3′), sirtuin 3 (SIRT3) (Forward: 5′-TGC CAG CTT GTC TGA AGC A-3′ and Reverse: 5′-GTC CAC CAG CCT TTC CAC A-3′), BAX (Forward: 5′-AGG ATG CGT CCA CCA AGA AGC T-3′ and Reverse: 5′-TCC GTG TCC ACG TCA GCA ATC A-3′), Caspase 3 (Forward: 5′-GGA GTC TGA CTG GAA AGC CGA A-3′ and Reverse: 5′-CTT CTG GCA AGC CAT CTC CTC A-3′), PARP1 (Forward: 5′-GGA AAG GGA TCT ACT TTG CCG-3′ and Reverse: 5′-TCG GGT CTC CCT GAG ATG TG-3′), and GAPDH (Forward: 5′-AGG TCG GTG TGA ACG GAT TTG-3′ and Reverse: 5′-GGG GTC GTT GAT GGC AAC A-3′).

Gene expression analysis by NanoString technologies

Only male mice were included in the experiments. NanoString analysis was performed on the cochlear and auditory cortex

tissues from WT (n = 3), Polβ$^{+/-}$ (n = 3), 3xTgAD (n = 3), and 3xTgAD/Polβ$^{+/-}$ (n = 3) mice using a mouse metabolic pathway panel with 768 genes and 20 internal reference genes (XT-CSO-MMP1–12). Total RNA was purified with a PureLink™ RNA Mini Kit (Thermo Fisher Scientific, #12183018A) as per the manufacturer's protocol and quantified using a NanoDrop ND-1000 spectrophotometer. Purified RNA was diluted in nuclease-free water to 20 ng/uL. It was hybridized in a CodeSet mix carrying hybridization buffer, Reporter Code Set, and Capture Probe Set at 65 °C for 16–24 hours in a thermal cycler. Hybridized samples were loaded onto the nCounter Prep Station for immobilization in the sample cartridge (NanoString Technologies, MAN-C0035). The Prep Station can process up to 12 samples per run in approximately 2.5–3 hours, depending on which protocol was used. Next, the nCounter Digital Analyzer, which was a multichannel epifluorescence scanner, collected data by taking images of the immobilized fluorescent reporters in the sample cartridge with a CCD camera through a microscope objective lens. The results were downloaded from the nCounter Digital Analyzer in RCC file format. NanoString readout was analyzed via the NanoString nCounter nSolver 4.0 software (MAN-C0019-08) with the NanoString Advanced Analysis 2.0 plug-in (MAN-10,030-03) following the NanoString Gene Expression Data Analysis Guidelines (MAN-C0011-04). Both positive control and housekeeping normalization were used to normalize all sources of variation associated with the platform. Detection thresholds were established at the Log2 ratio relative to the reference (Log2 fold change). A fold-change cutoff of 1.5 was used. A p-value less than 0.05 and genes with a fold change of 1.5 were considered statistical significance. NanoString pathway score analysis was calculated as the expression values of constituent genes of each pathway via the NanoString nCounter nSolver 4.0 software. They were oriented such that an increasing score corresponds to mostly increased gene expression.

Statistical analysis

All data were analyzed by the Graph Pad Prism 8 software (San Diego, CA), and statistical significance was determined by one-way and two-way ANOVA analysis of variance with Tukey's multiple comparisons test, as appropriate. Results are presented as the mean ± standard deviation. The numbers of mice used in the various experiments are denoted in the figure legends. Differences were considered statistically significant with $*p < 0.05$ and $**p < 0.01$.

Results

Auditory impairment in 3xTgAD and 3xTgAD/Polβ$^{+/-}$ mice

The 3xTgAD mice develop age-dependent Aβ plaques, intraneuronal tau tangles, and cognitive deficits but do not exhibit neuronal death[23,33]. To investigate the impact of DNA damage and/or repair in the etiology of AD, we crossed DNA polymerase β heterozygous mice (Polβ$^{+/-}$) into the 3xTgAD mouse model to generate a DNA repair-deficient AD mouse (3xTgAD/Polβ$^{+/-}$) that has major features of human AD, including phosphorylated tau pathologies, neuronal death, and increased cognitive impairment[33,34]. Our previous studies have shown that the 3xTgAD/Polβ$^{+/-}$ mice accumulate more DNA damage and exhibit neuronal death in brain regions[33]. Thus, the 3xTgAD/Polβ$^{+/-}$ mouse has many humanized features compared to 3xTgAD. We first characterized the hearing function in four different mouse models (WT, Polβ$^{+/-}$, 3xTgAD, and 3xTgAD/Polβ$^{+/-}$) by ABR recordings (**Fig. 1A**). ABR assay is a neurologic test of auditory brainstem function in response to auditory stimulus. With electric potential, five to seven waves are recorded in the first 10 ms due to the synchronous firing of nerve fibers after an auditory stimulus. We found that 3xTgAD and 3xTgAD/Polβ$^{+/-}$ mice had significantly higher thresholds than WT mice at frequencies between 16 and 32 kHz as early as 4 weeks of age (**Fig. 1B,C**). Interestingly, ABR thresholds in 3xTgAD/Polβ$^{+/-}$ male mice were significantly increased compared to 3xTgAD male mice at 16 kHz (**Fig. 1B**) but not in female mice (**Fig. 1C**). To further characterize the hearing loss in 3xTgAD and 3xTgAD/Polβ$^{+/-}$ mice, we analyzed their ABR waveforms, labeled from I to VII[46]. The two first waves (waves I and II) are known to be generated from auditory nerves[47,48]. Waves III–V come from the higher components of the pathway, such as the cochlear nucleus, superior olivary complex, lateral lemniscus, and inferior colliculus. The last two waves (waves VI and VII) are considered to come from the thalamus. As shown in **Figure 1**, a reduction in wave magnitude or increase in wave latency indicates a hearing deficit; thus, the impacted wave provides valuable information for locating deficits along the auditory pathway. We observed significant differences in 3xTgAD and 3xTgAD/Polβ$^{+/-}$ mice when compared to the waves of WT and Polβ$^{+/-}$ mice. Interestingly, male 3xTgAD and 3xTgAD/Polβ$^{+/-}$ mice had significantly lower wave I amplitudes. In females, the difference between WT and 3xTgAD mice was not significant (p-value 0.0624), but the difference between 3xTgAD/Polβ$^{+/-}$ mice and WT was significant (**Fig. 1D,E**). The delay of the latency of wave I, also indicative of a hearing deficit, showed a similar pattern as their amplitudes. Male 3xTgAD and 3xTgAD/Polβ$^{+/-}$ mice had increased latency compared to WT, whereas latencies in females were changed significantly only in 3xTgAD/Polβ$^{+/-}$ mice (**Fig. 1F,G**). Together, these results show that hearing impairment can be detected in 3xTgAD and 3xTgAD/Polβ$^{+/-}$ mice as early as 4 weeks of age, indicating very early hearing loss in mouse models of AD. Notably, our findings show earlier hearing loss than reported in previous studies[21,22]. We next assessed auditory capacity with DPOAE, which provides information about cochlear integrity and outer hair cell function. Loss of outer hair cells causes loss of sensitivity and frequency discrimination (see the Methods section for details). As shown in **Figure 1H**, 3xTgAD and 3xTgAD/Polβ$^{+/-}$ male mice at 4 weeks of age had lower DPOAE signals than WT mice at 16 kHz, but this was not the case in female mice (**Fig. 1I**). There were also no significant reductions at 10, 12, 24, and 32 kHz (**Supplementary Fig. 1**). Thus, we detect a loss of outer hair cell function in 3xTgAD and 3xTgAD/Polβ$^{+/-}$ male mice at 16 kHz, and these results also collectively show that male mice are more susceptible to hearing impairment than females.

3xTgAD/Polβ$^{+/-}$ mice have a decreased number of ribbon synapses

The cochlea is composed of base, middle, and apex regions; the base region senses high-frequency and the apex region senses low-frequency sounds[45]. The loss of hair cells and IHC synapses in each area of the cochlea strongly correlate with the loss of hearing function at the corresponding frequency ranges. To quantify hair cells and synapses in the cochlea, we dissected whole-mount organ of Corti tissue and stained with vGlut3 (IHCs), anti-CtBP2 (pre-synapse), and anti-Homer1 (postsynapse) (**Fig. 2A–C**). Immunolabeling was quantified in a blinded fashion by counting

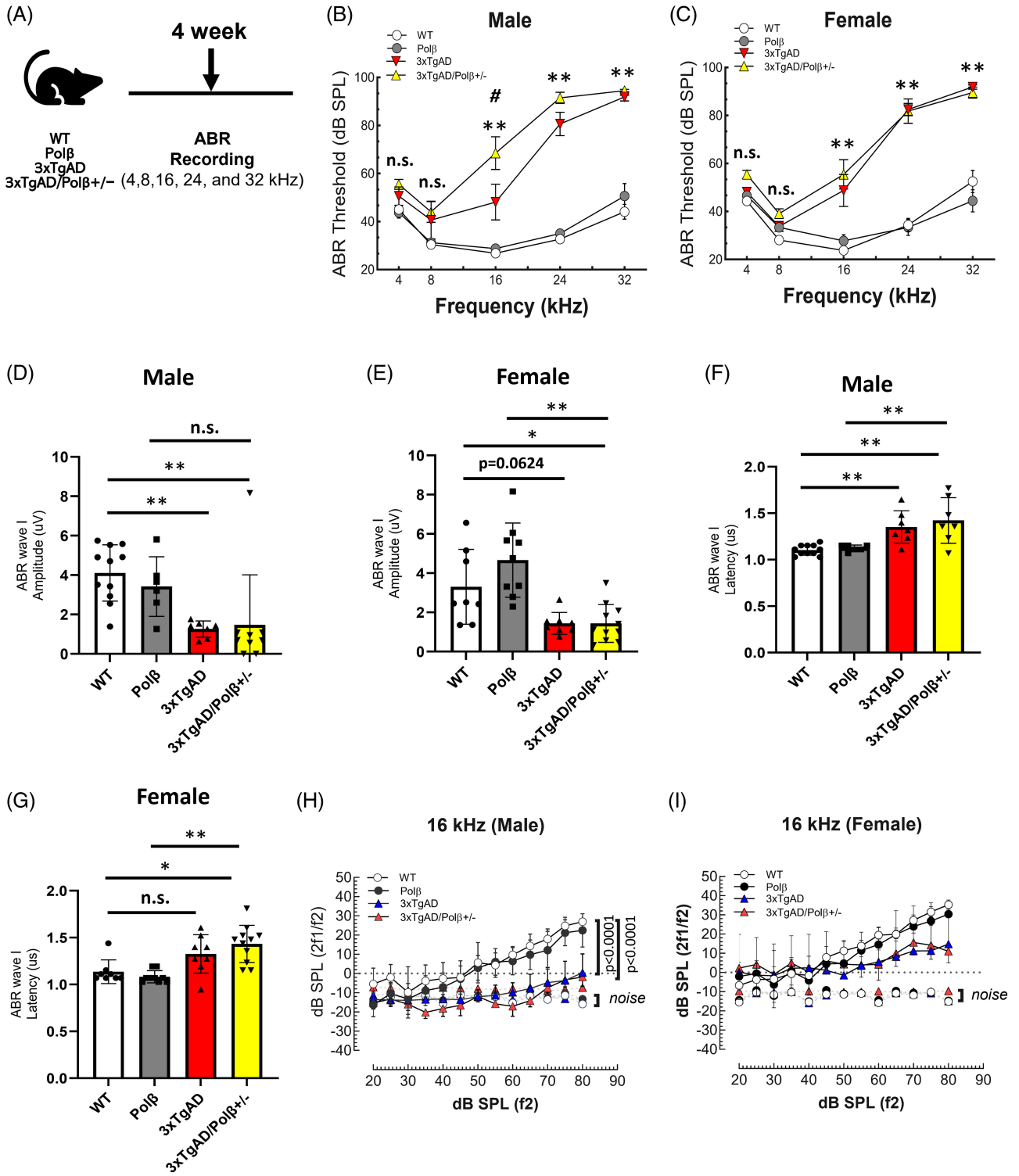

Figure 1. Hearing loss in 3xTgAD and 3xTgAD/Polβ$^{+/-}$ mice. (A) Experiment scheme for auditory brainstem response (ABR) recordings at 4 weeks of age in the 4, 8, 16, 24, and 32 kHz. WT, Polβ$^{+/-}$, 3xTgAD, and 3xTgAD/Polβ$^{+/-}$ mice were used. **(B)** ABR threshold in male mice. **(C)** ABR threshold in female mice. Significant elevation of ABR thresholds was observed at 4 weeks of age in 3xTgAD and 3xTgAD/Polβ$^{+/-}$ mice. In male, ABR thresholds between 3xTgAD and 3xTgAD/Polβ$^{+/-}$ mice were significantly different at 16 kHz. **(D,E)** Quantification of the amplitude of wave I in each group at 16 kHz and 90 dB. **(F,G)** Quantification of the latency of wave I in each group at 16 kHz and 90 dB. The dots represent individual mice. **(H)** Distortion product otoacoustic emission (DPOAE) recordings in male mice and **(I)** DPOAE recordings in female mice. A significant reduction of DPOAE signals at 16 kHz was observed at 4 weeks of age in 3xTgAD and 3xTgAD/Polβ$^{+/-}$ male mice but not in female mice. n = 7–11 mice per group. *p < 0.05, **p < 0.01, 3xTg and 3xTgAD/Polβ$^{+/-}$ mice compared to WT mice. #p < 0.05, 3xTgAD/Polβ$^{+/-}$ mice compared to 3xTg mice. Two-way ANOVA with Tukey's multiple comparisons test. Error bars represent the mean ± standard deviation (SD).

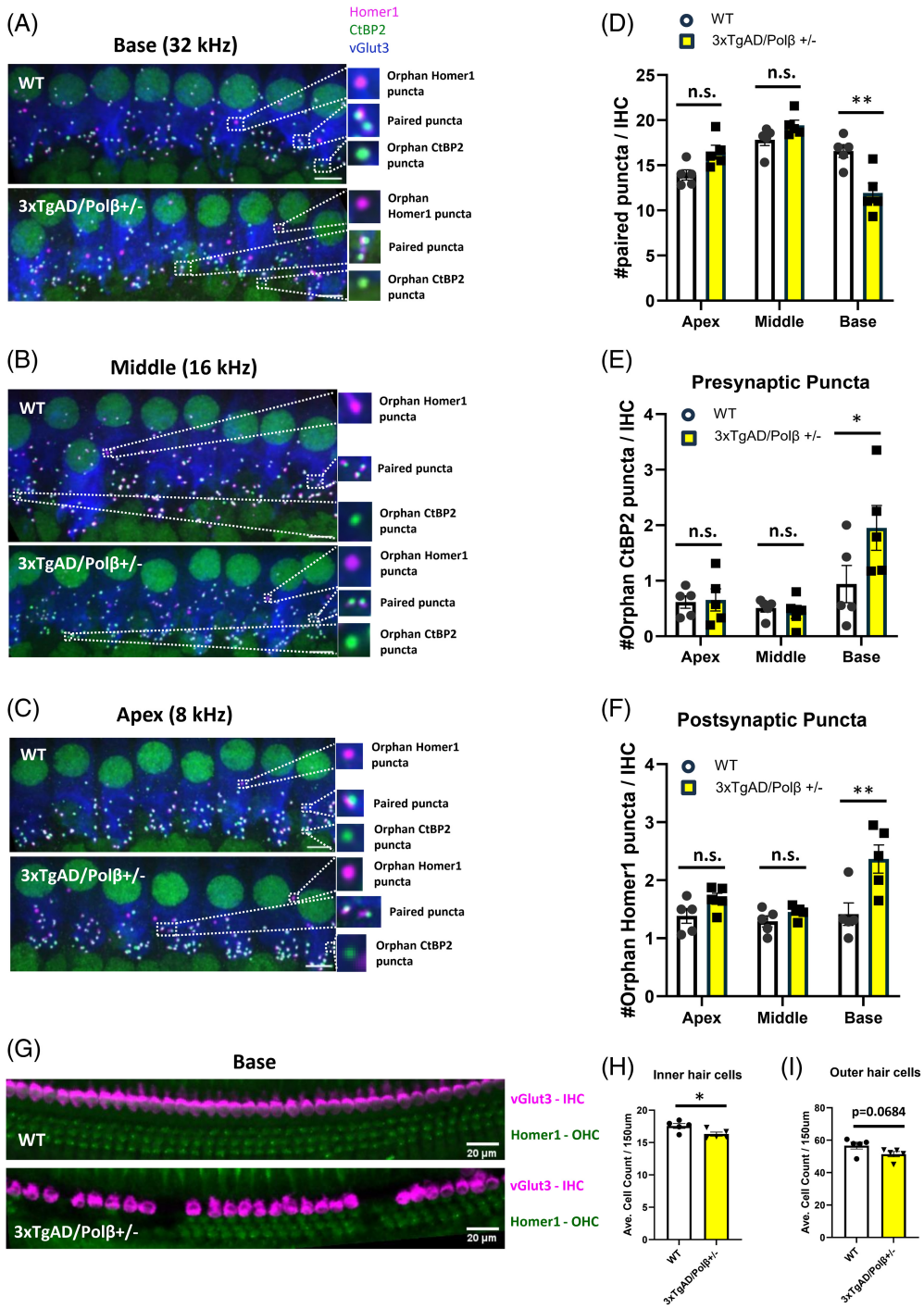

Figure 2. DNA damage in the cochlea induces defects in functional synapses in 3xTgAD/Polβ$^{+/-}$ mice. **(A–C)** Representative image of immunostaining for synaptic ribbons in the apex (8 kHz), middle (16 kHz), and base (32 kHz) regions of the cochlea in WT and 3xTgAD/Polβ$^{+/-}$ mice at 4 weeks of age. A magnification of 100× was used for all images. **(D)** Quantitative analysis of paired puncta per inner hair cell (IHC) in the cochlea at 8, 16, and 32 kHz. The average number of paired puncta is reduced in 3xTgAD/Polβ$^{+/-}$ mice relative to WT mice. **(E,F)** The graphs show the average number of orphan ribbons per IHC at 8, 16, and 32 kHz. The green puncta (anti-Ctbp2) and the magenta puncta (anti-Homer1). Each puncta represents a single synaptic ribbon in an individual mouse. **(G)** Representative images of base inner and outer hair cells of WT and 3xTgAD/Polβ$^{+/-}$ mice at 4 weeks of age. A magnification of 20× was used for the hair cell image. **(H,I)** The average number of inner and outer hair cells per 150 µm in the basal region of the cochlea in WT or 3xTgAD/Polβ$^{+/-}$ mice. The number of IHCs decreased in 3xTgAD/Polβ$^{+/-}$ mice. In contrast, there were no significant changes in the number of outer hair cells. n = 5 male mice per group. *p < 0.05, **p < 0.01, two-way ANOVA with Tukey's multiple comparisons test. Error bars represent the mean ± SD.

paired ribbon-forming punctae in IHCs of WT and 3xTgAD/Polβ$^{+/-}$ male mice. Compared to WT mice, 3xTgAD/Polβ$^{+/-}$ male mice showed a significant reduction in paired ribbon synapses of IHCs in the 32 kHz region of the cochlea, suggesting a loss of functional synapses in the DNA repair-deficient AD mouse model (Fig. 2D). For hair cell quantification, we analyzed 20× regions within each third (apex, middle, and base) of WT and 3xTgAD/Polβ+/− cochleae (**Supplementary Fig. 2a**). The number of

orphan punctae immunolabeled with CtBP2 and Homer1 in IHCs of WT and 3xTgAD/Polβ$^{+/-}$ male mice was quantified at 32 kHz. We found an increase in the number of orphan CtBP2 and Homer1 puncta, specifically in the 32 kHz region of 3xTgAD/Polβ$^{+/-}$ male mice (Fig. 2E,F). The number of orphan punctae in the 8 and 16 kHz regions remained unaffected, suggesting that there was no synaptopathy in these regions at this age (Fig. 2E,F). We next analyzed the number of inner and outer hair cells in the base, middle, and apex regions of the cochlea in WT and 3xTgAD/Polβ$^{+/-}$ male mice. There were significantly fewer IHCs in the basal cochlear region in 3xTgAD/Polβ$^{+/-}$ male mice than in WT (Fig. 2G,H), while the middle and apex regions were largely unaffected (**Supplementary Fig. 2**). The outer hair cell number tended to be reduced in the base of the cochlea region in 3xTgAD/Polβ$^{+/-}$ male mice (p-value 0.0684) (Fig. 2I). The number of paired ribbon synapses and total number of hair cells at the 8 and 16 kHz regions were not reduced in the 3xTgAD/Polβ$^{+/-}$ male mice compared to the WT male mice (Fig. 2D and **Supplementary Fig. 2b,c**). These data are consistent with the ABR data showing high-frequency hearing loss in 3xTgAD/Polβ$^{+/-}$ mice and decreased wave I amplitudes, which correlate with the observed synaptopathy in the corresponding regions.

Increased DNA damage in the cochlea is associated with NAD$^+$ decline

To investigate the mechanism of this early hearing loss found in the AD mice, we performed gene expression analysis by NanoString Technologies using the mouse cochlea[49] and auditory cortex[50] (Fig. 3A) from 3xTgAD and 3xTgAD/Polβ$^{+/-}$ male mice. Since the auditory cortex is the most highly organized sound-processing unit in the brain, we chose the auditory cortex, which is located in a region close to the cochlea, for comparison and investigated gene expression changes in the cochlea and auditory cortex. We employed the Metabolic Pathways Panel. Significantly changed pathways were defined as those displaying an absolute z-score of at least 1.5. Genes with a fold change of 1.5 were considered statistically significant. Heatmap analysis showed significant differences between the cochlea and the auditory cortex (Fig. 3A). Notably, one of the most significantly altered terms in the cochlea was DNA damage repair. When compared to age-matched male WT, DNA damage repair was highly downregulated in Polβ, 3xTgAD, and 3xTgAD/Polβ$^{+/-}$ male mice (Fig. 3B). We next examined the DNA damage markers in cochlea and auditory cortex tissue. Poly (ADP-ribose) (PAR) polymerase 1 (PARP1) is an enzyme predominantly activated in response to DNA damage and modifies proteins by a process known as PARylation, a posttranslational modification process with key roles in DNA repair and metabolism. PARylation regulates chromatin organization, DNA repair, transcription, and replication. PARP1 is activated by DNA damage, has a major role in DNA repair, and participates in several cellular processes[51,52]. Compared with WT male mice, there was an increase in PAR and PARP1 in the cochlea of 3xTgAD and 3xTgAD/Polβ$^{+/-}$ male mice (Fig. 3E,F and **Supplementary Fig. 3**), which was accompanied by increased phosphorylation of H2AX at Ser 139 (γ-H2AX), indicative of an induction of double-strand breaks. Interestingly, the levels of γ-H2AX in the cochlea between 3xTgAD and 3xTgAD/Polβ$^{+/-}$ male mice were significantly different (Fig. 3C,G), while the auditory cortex was largely unaffected (Fig. 3D,J).

Next, multiple signaling pathway scores in the nanostring analysis were explored in the cochlea and auditory cortex. Interestingly, pathways involved in cell death, oxidative stress, reactive oxygen species, autophagy, mitogen activated protein kinase, and AMP-activated protein kinase were significantly upregulated in the cochlea (**Supplementary Fig. 4a–d**), but not in the auditory cortex (**Supplementary Fig. 4e–h**) of 3xTgAD and 3xTgAD/Polβ$^{+/-}$ male mice, suggesting that DNA damage in the cochlea-induced signaling pathways involved in cellular damage. Nicotinamide adenine dinucleotide (NAD) is a coenzyme central to metabolism, which also plays vital roles in DNA repair, cell metabolism, and cell survival[53]. The decline in NAD$^+$ levels may result in inadequate DNA repair and mitochondrial dysfunction in AD[34], and is linked to hearing loss in Cockayne syndrome[45]. Many of these aging-associated diseases can be improved by restoring NAD$^+$ levels[53]. To identify how NAD$^+$ levels change in the cochlea and auditory cortex, the NAD$^+$ levels were measured and compared with WT mice. As shown in Figure 3K, a significant relative decline in NAD$^+$ levels was detected in the cochlea, whereas there was no decline in the auditory cortex tissues at 4 weeks of age.

To further investigate whether DNA damage in the cochlea directly impacts hearing loss, we examined hearing loss induced by gamma irradiation (IR). Male and female WT and 3xTgAD/Polβ$^{+/-}$ mice were subjected to whole-body IR in a Nordion Gamma cell 40 Exactor Irradiator. IR (6 Gy) was delivered at a rate of 0.74 Gy/min. As shown in Figure 4A, immediately after IR exposure (4 hours), the ABR threshold in male mice was significantly increased in 3xTgAD/Polβ$^{+/-}$ mice but not in WT at 16 Hz (Fig. 4B). In female mice, the ABR threshold was also slightly higher in 3xTgAD/Polβ$^{+/-}$ mice exposed to IR; however, there was no significant difference at 16 Hz (Fig. 4C). This observation was consistent with the ABR data showing hearing loss in between 3xTgAD and 3xTgAD/Polβ$^{+/-}$ male mice (Fig. 1B). We detected significantly increased levels of γ-H2AX in the cochlea of WT and 3xTgAD/Polβ$^{+/-}$ male mice compared to the auditory cortex, indicating that the cochlea responds earlier to DNA damage than the auditory cortex (Fig. 4D–G).

DNA damage in the cochlea is associated with Pgam2 reduction

To further explore the molecular mechanisms of hearing loss in AD, we analyzed significantly changed genes from the cochlea and auditory cortex of 3xTgAD and 3xTgAD/Polβ$^{+/-}$ male mice compared with WT. According to the NanoString metabolic pathway panel, the following genes were significantly changed: *Apoc3*, *Hnf4a*, *Ngfr*, *Alox15*, *Gck*, *Pgam2*, *Zap70*, *Gzmd*, and *Slc2a5*. Among these, Pgam2, which is a glycolytic enzyme, was notably downregulated in the cochlea (Fig. 5A). Interestingly, we observed a similar trend of decreases in protein (Fig. 5B,D) and mRNA (Fig. 5E) levels of Pgam2 in the cochlea of male mice. The quantitative measurement of Pgam2 (Fig. 5F) and Eno3 (Enolase 3) levels, a Pgam2-interacting protein, showed a decrease in the cochlea of 3xTgAD and 3xTgAD/Polβ$^{+/-}$ male mice (**Supplementary Fig. 5a,b**). We also explored the expression of Pgam2 in female mice. Western blot analysis showed no significant difference in the cochlea of these mice (**Supplementary Fig. 5c,d**). There was also no significant change in Pgam2 (Fig. 5C,H,I,J) and Eno3 levels (**Supplementary Fig. 5c,d**) in the auditory cortex compared with WT male mice. T-box transcription factor 2 (Tbx2) is an essential transcription factor in the process of hair cell development and regeneration in the cochlea[54]. It was downregulated in the cochlea of 3xTgAD/Polβ$^{+/-}$

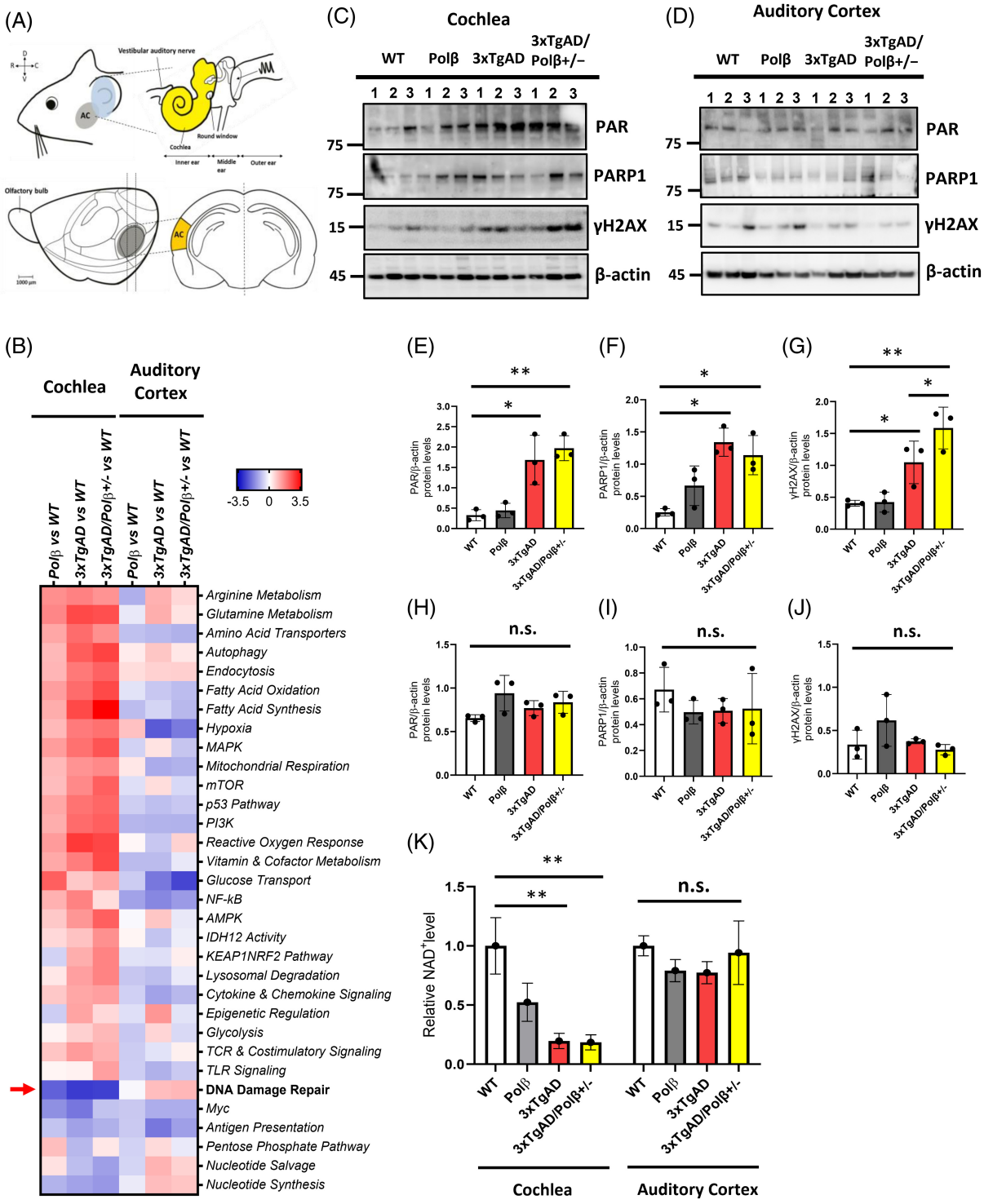

Figure 3. DNA damage is accumulated in the cochlea. **(A)** Schematic drawing of the mouse cochlea and auditory cortical regions for recording. **(B)** Heatmap of pathways from NanoString analysis in the cochlea and auditory cortex. Significant pathways with a fold change of ≥1.5 from each comparison relative to WT. The heatmap shows significantly downregulated DNA damage repair pathways in the cochlea. **(C,D)** Representative western blots showing PAR, PARP1, and γH2AX in the cochlea and auditory cortex. **(E–J)** Quantification of PAR, PARP1, and γH2AX protein levels in the cochlea and auditory cortex. The γH2AX band was normalized to loading controls β-actin. AC denotes the auditory cortex. **(K)** Relative NAD^+ levels were measured in the cochlea and auditory cortex of WT, $Pol\beta^{+/-}$, 3xTgAD, and 3xTgAD/$Pol\beta^{+/-}$ mice at 4 weeks of age. n = 3 male mice per group. Note: The ratio of NAD^+/NADH in WT mice was lower in the auditory cortex compared with the cochlea. NAD^+/NADH levels were normalized to total protein. *p < 0.05, **p < 0.01, two-way ANOVA with Tukey's multiple comparisons test. Error bars represent the mean ± SD.

male mice compared with WT male mice. Of note, Tbx2 protein expression in cochlea was significantly different between 3xTgAD and 3xTgAD/$Pol\beta^{+/-}$ male mice (Fig. 5B,G), while auditory cortex it was unaffected (Fig. 5C,K). Together, these data suggest that the cochlea is an early-affected organ in AD and that reduced Pgam2 may be associated with hearing loss in AD mice.

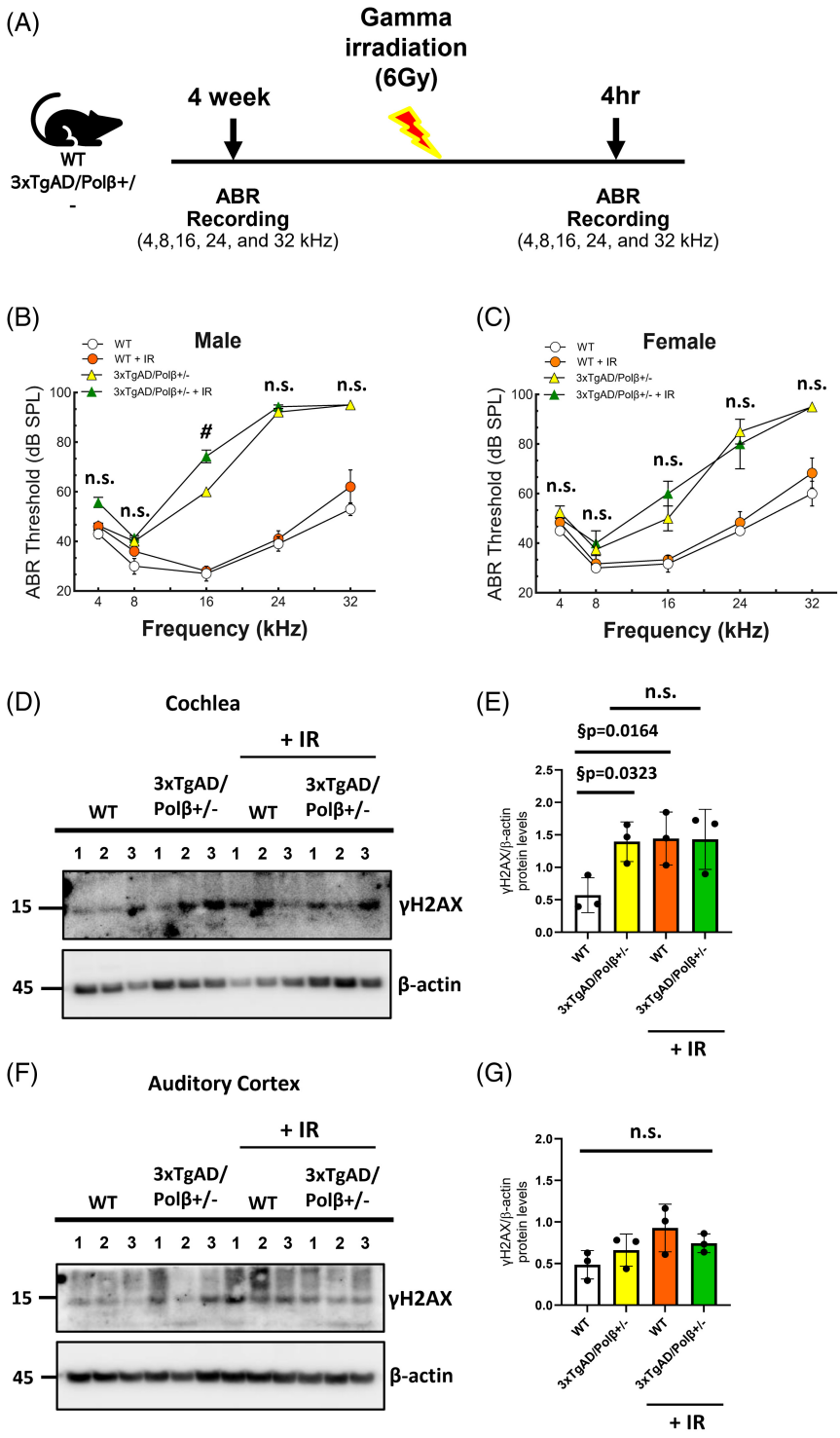

Figure 4. Increased DNA damage may affect the hearing adversely. **(A)** Outline for irradiation (IR) treatment and ABR recordings at 4 weeks of age in WT and 3xTgAD/Polβ$^{+/-}$ mice. **(B)** ABR threshold in male mice. **(C)** ABR threshold in female mice. n = 3–4 mice per group. **(D,F)** Representative western blots showing γH2AX in the cochlea and auditory cortex of WT and 3xTgAD/Polβ$^{+/-}$ male mice. **(E,G)** Quantification of γH2AX protein levels in the cochlea and auditory cortex. n = 3 mice per group. The γH2AX band was normalized to loading controls β-actin. #$p < 0.05$, IR-treated 3xTgAD/Polβ$^{+/-}$ mice compared to 3xTgAD/Polβ$^{+/-}$ mice. Two-way ANOVA with Tukey's multiple comparisons test. Error bars represent the mean ± SD. Note: §p is the p value obtained with the student's t-test as the two-way ANOVA analysis did not quite reach significance of $p < 0.05$.

Accumulation of DNA damage and downregulation of mitochondrial SIRT3 levels in the cochlea increase the acetylation of SOD2

Mitochondrial SIRT3, the NAD^+-dependent deacetylase, plays an important role in hair cell survival by regulating mitochondrial function[31,55], modulating reactive oxygen species, and limiting oxidative damage to cellular components[56–58]. We hypothesized that SIRT3 alteration in the cochlea may be involved in the hearing loss in AD. We thus assessed the level of SIRT3 in Polβ, 3xTgAD, and 3xTgAD/Polβ$^{+/-}$ male mice. Western blot

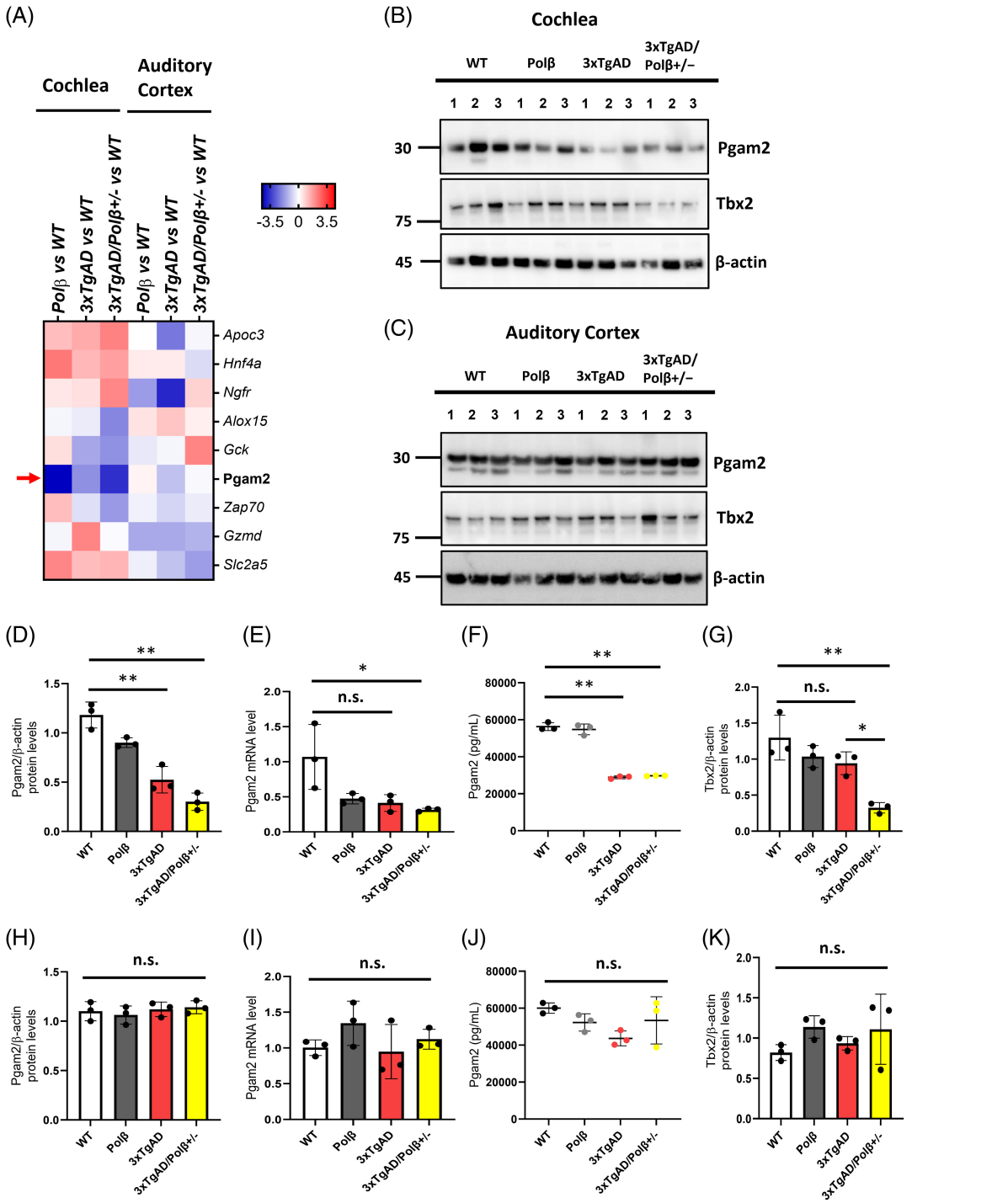

Figure 5. Phosphoglycerate mutase 2 (Pgam2) is downregulated in the cochlea of 3xTgAD and 3xTgAD/Polβ$^{+/-}$ mice. **(A)** Heatmap of gene expression from NanoString analysis in the cochlea and auditory cortex. **(B,C)** Representative western blots show Pgam2 and Tbx2 in the cochlea and auditory cortex. **(D,H)** Quantification of Pgam2 protein levels in the cochlea and auditory cortex. **(E,I)** Quantitative real-time PCR (qPCR) analysis for the relative gene expression of Pgam2 in the cochlea and auditory cortex. **(F,J)** Quantitative measurement of Pgam2 levels in the cochlea and auditory cortex. **(G,K)** Quantification of Tbx2 protein levels in the cochlea and auditory cortex. Pgam2 and Tbx2 bands were normalized to loading controls β-actin. n = 3 male mice per group. *$p < 0.05$, **$p < 0.01$, two-way ANOVA with Tukey's multiple comparisons test. Error bars represent the mean ± SD.

(Fig. 6A,B) and qPCR (Fig. 6D) analyses showed significantly reduced expression of SIRT3 in the cochlea of AD male animals compared to WT mice but no significant difference in the auditory cortex (Fig. 6G,H,J). We next examined the protein expression of SIRT3 in female mice. SIRT3 expression tended to decrease in Polβ, 3xTgAD, and 3xTgAD/Polβ+/− female mice, but did not reach significance (**Supplementary Fig. 6**). SIRT3 is a major mitochondrial deacetylase, and we next measured its activity by the acetylation state of its known substrate, superoxide dismutase 2 (SOD2), in cochlea and auditory cortex samples. Acetylated SOD2 (K68) was significantly increased in the cochlea of 3xTgAD and 3xTgAD/Polβ$^{+/-}$ male mice compared to WT (Fig. 6C),

indicating reduced SIRT3 activity. Notably, acetylated SOD2 was significantly increased in 3xTgAD/Polβ$^{+/-}$ male mice in the auditory cortex (Fig. 6I) and in female mice as well (**Supplementary Fig. 6**). In the absence of SIRT3, there is increased oxidative stress, impairment of mitochondrial function, and apoptosis under stress[59]. Thus, we explored expression of the apoptosis-related proteins, BAX and Caspase-3, in the cochlea and auditory cortex of 3xTgAD and 3xTgAD/Polβ$^{+/-}$ male mice. The results demonstrated that mRNA levels of these proteins in the cochlea were significantly increased in 3xTgAD/Polβ$^{+/-}$ male mice compared with WT, but not in 3xTgAD male mice (Fig. 6E,F). While we detected a decrease in SIRT3 levels in the cochlea, we did not

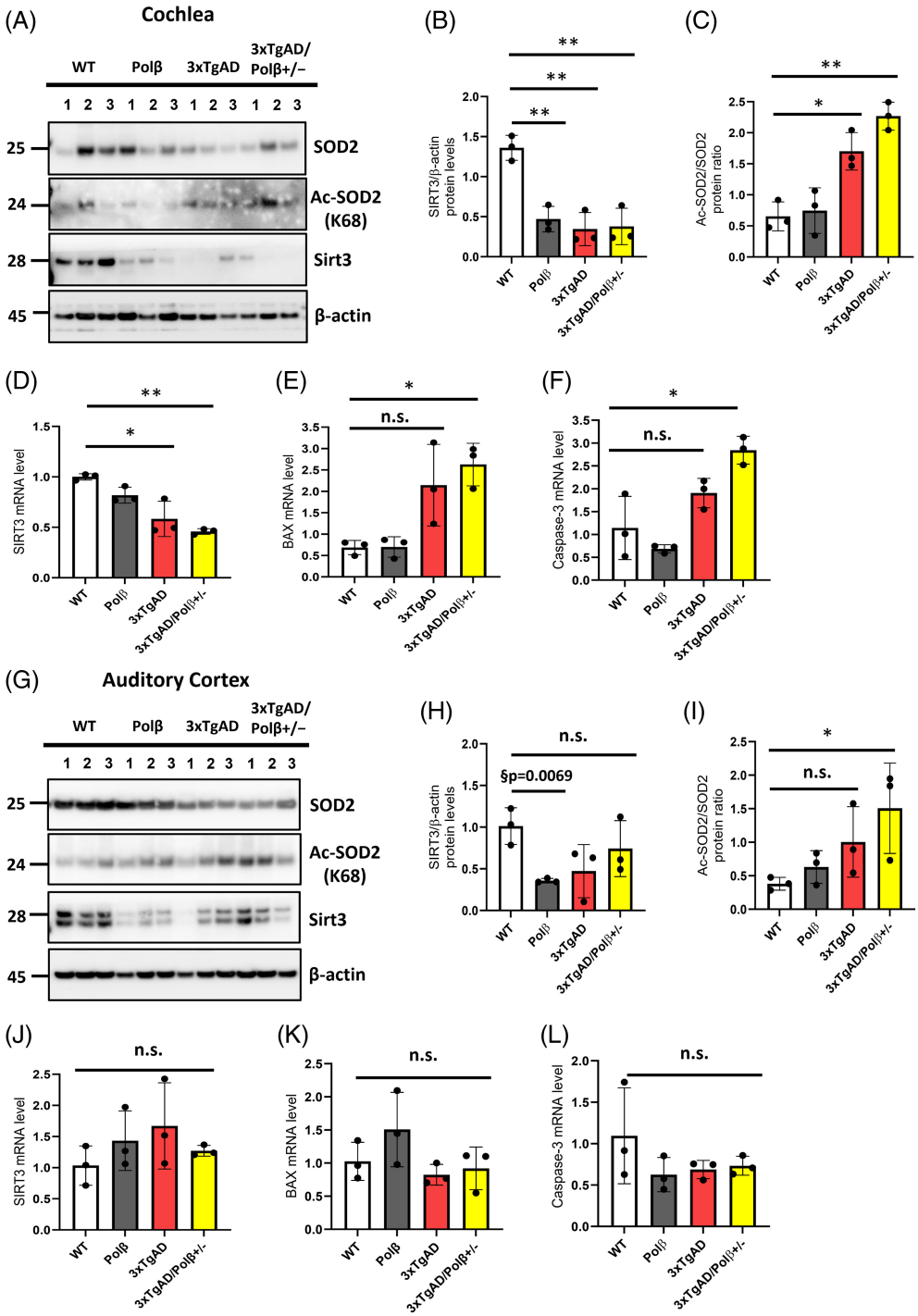

Figure 6. Increased DNA damage decreases sirtuin 3 (SIRT3) levels in the cochlea of 3xTgAD and 3xTgAD/Polβ$^{+/-}$ mice. **(A,G)** Representative western blots show SIRT3, SOD2, and Ac-SOD2 (acetyl K68) in the cochlea and auditory cortex. **(B,C,H,I)** Quantification of SIRT3 and Ac-SOD2 (acetyl K68) protein levels in the cochlea and auditory cortex. **(D–F,J–L)** qPCR analysis for the relative gene expression of SIRT3, BAX, and Caspase-3 in the cochlea and auditory cortex. n = 3 male mice per group. The Ac-SOD2 band was normalized to total SOD2. The other bands were normalized to loading controls β-actin. *$p < 0.05$, **$p < 0.01$, two-way ANOVA with Tukey's multiple comparisons test. Error bars represent the mean ± SD. Note: $^{§}p$ is the p value obtained with the student's t-test.

observe a similar difference in the auditory cortex (Fig. 6K,L). Together, these results suggest that SIRT3 downregulation in the cochlea may be associated with cochlear cell survival.

Discussion

In this study, we investigated hearing function in 3xTgAD and 3xTgAD/Polβ$^{+/-}$ mice. We first demonstrated that ABR thresholds are significantly increased between 16 and 32 kHz at 4 weeks of age in both 3xTgAD and 3xTgAD/Polβ$^{+/-}$ mice, many months before the earliest onset of behavioral changes in these mice (Fig. 7). One of the most significant findings in this study was that 3xTgAD and 3xTgAD/Polβ$^{+/-}$ mice show earlier hearing loss than previous studies in other AD mouse models[21,22]. Our data show that 3xTgAD and 3xTgAD/Polβ$^{+/-}$ mice have a significantly earlier onset of age-related hearing loss than WT, and this is consistent with the hypothesis that hearing impairment is an early biomarker of AD pathology. Here, it must be noted that both WT and 3xTgAD/Polβ$^{+/-}$ mice in this study have the CDH23 R72W mutation common in the C57/Bl6J background strain. This mutation accelerates both noise and age-related hearing loss, which can be a confounding factor but also a useful tool for studying progressive hearing loss phenotypes, which may otherwise have very long timelines.

For hearing analysis, ABR, an objective measurement of auditory pathway function from the auditory nerve to the mesencephalon, measures the neuronal electrophysiology in response to sound, and DPOAE quantifies the outer hair cell function in the cochlea. We investigated whether DNA damage or repair deficiency is associated with hearing loss in AD mice. We observe no significant differences at high frequencies (24–32 kHz) between 3xTgAD and 3xTgAD/Polβ$^{+/-}$ mice; however, as shown in Figure 1B, we observed that the ABR thresholds in the DNA repair-deficient, 3xTgAD/Polβ$^{+/-}$ mice were significantly increased compared to 3xTgAD mice, suggesting that Polβ DNA repair deficiency can be implicated in hearing loss. We also quantified the amplitudes of individual ABR waves in each mouse group (Fig. 1). The first wave (wave I) captures the activity of IHCs, afferent auditory neurons, synaptic transmission, and the synaptic connectivity between them[46–48]. Because wave amplitude is difficult to measure at low decibel sounds, we analyzed wave amplitude in response to higher decibel sounds (90 dB) to account for all mice, including those with prominent hearing dysfunction. We found that the average wave amplitude declined significantly at 4 weeks of age in both 3xTgAD and 3xTgAD/Polβ$^{+/-}$ mice compared to WT mice. We also quantified the wave latency, which is determined by the time between the initial auditory stimulus and the peak of a wave. As expected, the latency of wave I was delayed. The reduction in the wave magnitude and increase in wave latency indicate a hearing deficit and are correlated with synapse loss as measured by immunofluorescence imaging (Fig. 2). Together, our data indicate a deficit in the cochlear component of the auditory pathway, including hair cell and synapse loss. However, the hair cell and synapse loss were not sufficient to explain the magnitude of hearing loss, suggesting additional defects in other cell types and structures in the cochlea.

Here, we find that biological sex differences affect the hearing dysfunction of AD. The ABR thresholds in males are significantly higher in 3xTgAD/Polβ$^{+/-}$ mice than in 3xTgAD mice at 16 kHz, but not in female mice. Notably, the ABR waveforms, particularly wave I, showed a difference in 3xTgAD and 3xTgAD/Polβ$^{+/-}$ mice in both male and female. We observed that 3xTgAD and 3xTgAD/Polβ$^{+/-}$ male mice had increased latency compared to WT mice; however, latency in female was largely changed only in 3xTgAD/Polβ$^{+/-}$ mice (Fig. 1F,G). Furthermore, we found that DPOAE levels at 16 kHz in these male mice were significantly reduced compared with WT mice (Fig. 1H), but this was not the case in female mice (Fig. 1I). Consistent with previous studies[60,61], our results collectively showed that male mice are more susceptible to hearing impairment than females. It has been suggested that men are twice as likely to have hearing loss as women among adults aged 20–69[60]. The male cochlea was found to be longer than the female cochlea by approximately 1.11 mm. It has been hypothesized that variations in the cochlea length can influence the rigidity of the basilar membrane[61]. On the other hand, women are more likely than men to be diagnosed with any dementia, including AD[62]. While the mechanisms and causality of the gender-specific association for the relationship between hearing loss and AD remain unclear, a few theories have been proposed. Sex differences in hearing and dementia may result from hormonal differences between males and females[63]. Specifically, estrogen plays a significant role in both the development of the inner ear and the hearing process[64]. Furthermore, our previous research investigated whether biological sex impacts systemic metabolic alterations in 3xTgAD and 3xTgAD/Polβ$^{+/-}$ mice. Sex differences in brain mitochondrial metabolism were observed[65]. We found a mitochondrial complex I-specific impairment in cortical synaptic brain mitochondria in female AD mice but not male mice. In the

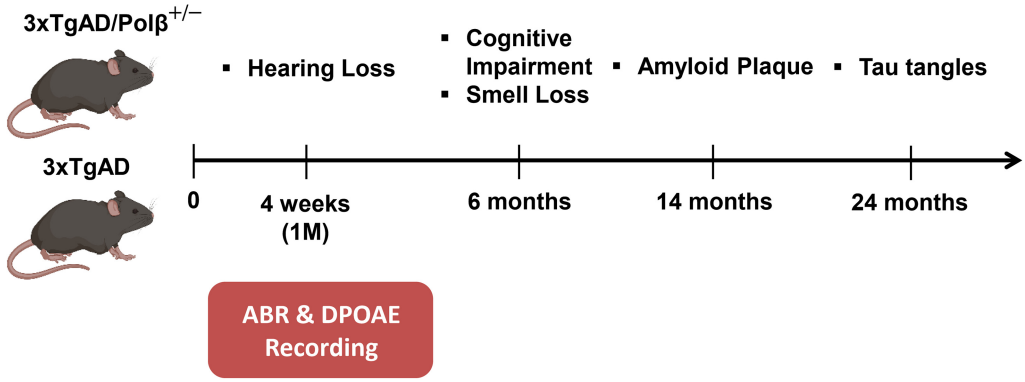

Figure 7. Schematic drawing of the time sequence of occurrence of hearing loss and typical Alzheimer's disease (AD) phenotypes in 3xTgAD and 3xTgAD/Polβ$^{+/-}$ mice. Hearing analyses (ABR and DPOAE) in the 3xTgAD and 3xTgAD/Polβ$^{+/-}$ mice were performed and significant elevation of ABR thresholds and reduction of DPOAE signal were observed at 4 weeks of age. Hearing impairment was much earlier than the occurrence of the AD phenotype, which appeared from 4 months of age. Cognitive impairment and smell loss (6 months). Amyloid plaque (14 months). Tau tangles (24 months).

hippocampus, Polβ haploinsufficiency caused synaptic complex I impairment in male and female mice[65]. Future studies investigating longitudinal changes to both the brain and cochlea of AD mice and humans will hopefully yield new insights into the sex-dependent relationship between hearing loss and dementia.

DNA damage accumulation is observed in the brains of AD patients and is well established as a significant causal factor in aging and neurodegeneration[36,37]. We compared two regions and identified an association between increased DNA damage and hearing loss in the cochlea and auditory cortex, which is the first region of the cerebral cortex to receive auditory inputs[66]. Auditory input arriving at the cochlea is transmitted through the auditory nerve to the cochlear nucleus, which is divided into dorsal and ventral regions in the brainstem. The superior olivary complex, traveling through several of its nuclei, receives input from the cochlear nucleus and has three nuclei involved in auditory input processing: the lateral superior olive, the medial superior olive, and the medial nucleus of the trapezoid body. The superior olivary complex then projects to the inferior colliculus in the midbrain through the fibers of the lateral lemniscus, synapsing in the lateral lemniscus nucleus. From the inferior colliculus, information travels to the medial geniculate body, which lies in the thalamus and is the last auditory center before reaching the auditory cortex, integrating information from several regions of the auditory system[66–68].

Compared to WT male mice, increased PAR, PARP1, and γ-H2AX were detected in the cochlea of 3xTgAD and 3xTgAD/Polβ$^{+/-}$ male mice at 4 weeks of age, whereas the auditory cortex was not significantly affected (**Fig. 3**). Interestingly, we also observed significant differences between the cochlea and the auditory cortex in diverse signaling pathways. In addition, a significant decline in NAD$^+$ levels was observed in the cochlea compared with the auditory cortex (**Fig. 3**). Of note, we found a potential mechanism through IR treatment indicating that DNA damage in the cochlea may be related to early hearing loss in AD mice. We found a significantly different DNA damage response to IR stress between the cochlea and cerebral cortex in 3xTgAD/Polβ$^{+/-}$ male mice. Changes in the audiometry of 3xTgAD/Polβ$^{+/-}$ male mice and an increase in phosphorylation of H2AX at Ser139 in the cochlea following IR stress suggest that the cochlea responds earlier to DNA damage than the auditory cortex (**Fig. 4**). Thus, evaluation of DNA repair markers indicates that the cochlea tissues might have less DNA damage repair capacity or a higher damage load than the auditory cortex.

It is thought that most hearing loss, both age-related and early-onset, is due to damage to components of the middle or inner ear. In mammals, hair cells lack regenerative capacity, and their death leads to permanent hearing loss and vestibular dysfunction[27–29,69]. We investigated potential underlying molecular mechanisms, including DNA damage and impairment of hair cells in early hearing loss. To address this, we performed gene expression analysis by NanoString Technologies in the cochlea and auditory cortex. According to the NanoString metabolic pathway panel, the Pgam2 gene was highly downregulated in the cochlea of 3xTgAD and 3xTgAD/Polβ$^{+/-}$ male mice compared to WT mice (**Fig. 5**). One of the significant findings was that the Pgam2 gene was significantly changed only in the cochlea of male mice and not in female mice (**Supplementary Fig. 6**). This finding is interesting because both Pgam2 and Eno3 are genes involved in the development of the inner ear sensory organs[70,71], and in humans, men tend to have higher rates of hearing loss than women at a similar age[60,72]. Pgam is involved in a critical energy-producing process known as glycolysis and gluconeogenesis, which catalyzes the transformation between 3-phosphoglycerate and 2-phosphoglycerate and is widely found in various tissues[73]. Pgam2 is mainly expressed in the muscle tissue (skeletal muscle and cardiac muscle) and is expressed highly at skeletal muscle development stages[74]. Pgam2-K176R mutation significantly impairs cell glycolysis, which is much involved in various tissues and degenerative disorders as well as mitochondrial dysfunction that causes lower basal oxygen consumption rates, spare respiratory capacity, proton leaks, and ATP production[74,75]. Notably, Pgam2 levels are downregulated in the prefrontal cortex of AβPP/PS1 mice brain[76]. Pgam2 is also associated with the development of the inner ear sensory organs[70,71]. We examined whether the expression of Pgam2 or the number of hair cells (inner and outer) declined in the cochlea of AD mice. The levels of Pgam2, IHCs, and the synaptic ribbon counts in the base regions were reduced in 3xTgAD/Polβ$^{+/-}$ male mice relative to WT male mice (**Figs. 2** and **5**). Despite the dramatic hearing loss, the number of outer hair cells was not significantly affected in the cochlea of 3xTgAD/Polβ$^{+/-}$ male mice; however, we found that the outer hair cell number tended to be reduced in the cochlea of the base region, and DPOAE levels in these mice were significantly reduced compared with WT mice (**Fig. 1H,I**). We also detected a significant difference in Tbx2 levels, which is an essential transcription factor in the process of hair cell development, in the cochlea between 3xTgAD and 3xTgAD/Polβ$^{+/-}$ male mice (**Fig. 5G**), indicating that DNA damage or DNA repair deficiency in the cochlea may impair developing ear hair cells, and it was also associated with early hearing impairment. In line with these findings, we suggest that a reduction in IHCs and a decrease of functional synapses, as well as downregulation of Pgam2, in the cochlea, might be contributing to early hearing loss in AD. However, the magnitude of hearing loss is not fully explained by the observed levels of synaptopathy or hair cell loss. Future studies are needed to identify key targets.

Mitochondrial health plays a key role in regulating the cellular functions of hair cells. It is widely considered that mitochondrial impairment leads to hearing loss and that hearing dysfunction is often observed in patients with mitochondrial disorders. Previous studies suggested that mitochondrial dysfunction is one of the potential risk factors for sensorineural hearing loss[77,78]. Our current work suggests that increased DNA damage in the cochlea of AD mice is associated with the impairment of hair cells. We show that Polβ$^{+/-}$, 3xTgAD, and 3xTgAD/Polβ$^{+/-}$ male mice expressed lower levels of SIRT3 than WT male mice in the cochlea and then examined the acetylation state of SOD2, a target protein for SIRT3, in maintaining mitochondrial function[79]. Interestingly, alterations in SIRT3 have been observed in the cochlea of male but not female mice (**Supplementary Fig. 6**), suggesting that biological sex differences might affect SIRT3 alteration in the cochlea. The ratio of acetylated SOD2 on lysine 68 to SOD2 was significantly increased in AD (**Fig. 6**), demonstrating reduced activity of SIRT3. Furthermore, an increase in oxidative stress, reactive oxygen species, autophagy, and upregulation of apoptosis-related proteins were observed in the cochlea of 3xTgAD and 3xTgAD/Polβ$^{+/-}$ male mice. The NAD$^+$-dependent mitochondrial SIRT3 has been reported to play an important role in maintaining mitochondrial integrity, energy metabolism, and regulating mitochondrial oxidative pathways[56,57]. Experimental evidence supports SIRT3's role in protection against hearing loss and hair cell dysfunction by regulating mitochondrial function. Administration of the NAD$^+$ precursor, nicotinamide riboside, can prevent spiral ganglia neurite degeneration and noise-induced hearing loss, which is mediated by SIRT3[80]. In vitro, increased SIRT3

expression protects cells from oxidative stress-induced cell death and inhibits apoptosis in age-related SGNs and hair cells[81]. SIRT3 overexpression reduced axonal degeneration induced by noise exposure[80] and significantly attenuated hair cell injury by activating SIRT3-mediated SOD2 deacetylation[31]. We suggest that decreased SIRT3 in the cochlea leads to impaired mitochondrial health and that this contributes to a decrease in the number of hair cells in the cochlea and increased hair cell damage by activating SOD2 acetylation. Interestingly, mitochondrial dysfunction has been shown to have particularly deleterious effects on the stria vascularis, which were not investigated in this study but perhaps should be prioritized for future investigations[82,83].

Collectively, our findings show the earliest hearing loss in AD mice reported so far, suggesting that hearing loss may be an earlier diagnostic measure compared with the occurrence of other AD features[21,22]. We found that the increased DNA damage in the cochlea was associated with a decreased number of ribbon synapses and with NAD^+ decline, Pgam2, and SIRT3 downregulation. Our results indicate that the DNA damage in the cochlea may be associated with the early-onset hearing loss in AD. Further studies will be necessary to address a potentially causal relationship between DNA damage accumulation and hearing loss.

Acknowledgments

We thank Alfred May and Tomasz Kulikowicz for performing IR operations. We thank Dr. Tracy Fitzgerald for her help in training for ABR waveform analysis.

Funding

This research was supported by the Intramural Research Program of NIA, NIH (V.A.B.) and by intramural grants to V.A.B. J.-H.P. was supported in part by funds from ChromaDex, Inc. U.M. is supported by NIA P30AG068635 (Nathan Shock Center), the David F. and Margaret T. Grohne Family Foundation, Core Grant application NCI CCSG (CA014195), NIDCD R01 DC021075-01, NSF NeuroNex Award (2014862), and the CZI Imaging Scientist Award (doi: 10.37921/694870itnyzk) from the Chan Zuckerberg Initiative DAF, an advised fund of Silicon Valley Community Foundation (funder doi: 10.13039/100014989).

Author Contributions

J.-H.P., V.A.B., and D.L.C. conceived and designed the study. J.-H.P. performed the measurements of ABR and DPOAE, and data analysis and wrote the article. B.D.S., K.P., and X.C. performed experiments for ELISA and qPCR analysis, and contributed to the interpretation of the data. J.-H.P., D.L.C., and M.G. collected mouse tissues. M.G., K.I., L.S., and E.C. performed cochlea dissection, whole-mount cochlea staining, and contributed to image acquisition. M.N.O. and W.C. contributed to constructive discussions for data analysis. J.-H.P., U.M., V.A.B., and D.L.C. edited the article and contributed to the interpretation of the results. All authors read and approved the final article.

Conflict of Interest Statement

V.A.B. had a material CRADA agreement with ChromaDex, Inc.

Data Availability Statement

The NanoString GEO accession number for the data reported in this article is GSE232205. The datasets generated during and/or analyzed during the current study are available from the corresponding author on reasonable request.

Supplementary Materials

Supplemental information can be found online at https://doi.org/10.59368/agingbio.20240025.

Accepted January 24, 2024
Published February 20, 2024

References

1. Bloom G.S. (2014). Amyloid-β and tau: The trigger and bullet in Alzheimer disease pathogenesis. *JAMA Neurol.* **71**(4), 505–508. PMID: 24493463; doi: 10.1001/jamaneurol.2013.5847.
2. Spillantini M.G., & Goedert M. (2013). Tau pathology and neurodegeneration. *Lancet Neurol.* **12**(6), 609–622. PMID: 23684085; doi: 10.1016/S1474-4422(13)70090-5.
3. Hammond T.C., Xing X., Wang C., Ma D., Nho K., Crane P.K., … Lin A.-L. (2020). β-amyloid and tau drive early Alzheimer's disease decline while glucose hypometabolism drives late decline. *Commun. Biol.* **3**(1), 352. PMID: 32632135; doi: 10.1038/s42003-020-1079-x.
4. Hebert L.E., Weuve J., Scherr P.A., & Evans D.A. (2013). Alzheimer disease in the United States (2010-2050) estimated using the 2010 census. *Neurology* **80**(19), 1778–1783. PMID: 23390181; doi: 10.1212/WNL.0b013e31828726f5.
5. Hou Y., Dan X., Babbar M., Wei Y., Hasselbalch S.G., Croteau D.L., & Bohr V.A. (2019). Ageing as a risk factor for neurodegenerative disease. *Nat. Rev. Neurol.* **15**(10), 565–581. PMID: 31501588; doi: 10.1038/s41582-019-0244-7.
6. Schuknecht H.F., & Gacek M.R. (1993). Cochlear pathology in presbycusis. *Ann. Otol. Rhinol. Laryngol.* **102**(1 Pt 2), 1–16. PMID: 8420477; doi: 10.1177/00034894931020S101.
7. Livingston G., & Costafreda S. (2023). Preventing dementia through correcting hearing: Huge progress but more to do. *Lancet Public Health* **8** (5), e319–e320. PMID: 37062297; doi: 10.1016/S2468-2667(23)00058-0.
8. Blackwell D.L., Lucas J.W., & Clarke T.C. (2014). Summary health statistics for U.S. adults: National Health Interview Survey, 2012. *Vital Health Stat.* **10**(260), 1–161. PMID: 24819891.
9. Li S., Cheng C., Lu L., Ma X., Zhang X., Li A., … Gao X. (2021). Hearing loss in neurological disorders. *Front. Cell. Dev. Biol.* **9**, 716300. PMID: 34458270; doi: 10.3389/fcell.2021.716300.
10. Swords G.M., Nguyen L.T., Mudar R.A., & Llano D.A. (2018). Auditory system dysfunction in Alzheimer disease and its prodromal states: A review. *Ageing Res. Rev.* **44**, 49–59. PMID: 29630950; doi: 10.1016/j.arr.2018.04.001.
11. Uhlmann R.F., Larson E.B., & Koepsell T.D. (1986). Hearing impairment and cognitive decline in senile dementia of the Alzheimer's type. *J. Am. Geriatr. Soc.* **34**(3), 207–210. PMID: 3950288; doi: 10.1111/j.1532-5415.1986.tb04204.x.
12. Grimes A.M., Grady C.L., Foster N.L., Sunderland T., & Patronas N.J. (1985). Central auditory function in Alzheimer's disease. *Neurology* **35** (3), 352–352. PMID: 3871922; doi: 10.1212/WNL.35.3.352.
13. Strouse A.L., Hall J.W., & Burger M.C. (1995). Central auditory processing in Alzheimer's disease. *Ear Hear.* **16**(2), 230–238. PMID: 7789674; doi: 10.1097/00003446-199504000-00010.
14. Mohr E., Cox C., Williams J., Chase T.N., & Fedio P. (1990). Impairment of central auditory function in Alzheimer's disease. *J. Clin. Exp. Neuropsychol.* **12**(2), 235–246. PMID: 2341553; doi: 10.1080/01688639008400970.

15. Kurylo D.D., Corkin S., Allard T., Zatorre R.J., & Growdon J.H. (1993). Auditory function in Alzheimer's disease. *Neurology* **43**(10), 1893–1893. PMID: 8413944; doi: 10.1212/WNL.43.10.1893.
16. Gates G.A., Karzon R.K., Garcia P., Peterein J., Storandt M., Morris J.C., & Miller J.P. (1995). Auditory dysfunction in aging and senile dementia of the Alzheimer's type. *Arch. Neurol.* **52**(6), 626–634. PMID: 7763213; doi: 10.1001/archneur.1995.00540300108020.
17. Iliadou V., & Kaprinis S. (2003). Clinical psychoacoustics in Alzheimer's disease central auditory processing disorders and speech deterioration. *Ann. Gen. Hosp. Psychiatry* **2**(1), 12. PMID: 14690547; doi: 10.1186/1475-2832-2-12.
18. Gates G.A., Anderson M.L., McCurry S.M., Feeney M.P., & Larson E.B. (2011). Central auditory dysfunction as a harbinger of Alzheimer dementia. *Arch. Otolaryngol. Head Neck Surg.* **137**(4), 390–395. PMID: 21502479; doi: 10.1001/archoto.2011.28.
19. Gates G.A., Beiser A., Rees T.S., D'Agostino R.B., & Wolf P.A. (2002). Central auditory dysfunction may precede the onset of clinical dementia in people with probable Alzheimer's disease. *J. Am. Geriatr. Soc.* **50**(3), 482–488. PMID: 11943044; doi: 10.1046/j.1532-5415.2002.50114.x.
20. Brenowitz W.D., Filshtein T.J., Yaffe K., Walter S., Ackley S.F., Hoffmann T.J., … Glymour M.M. (2020). Association of genetic risk for Alzheimer disease and hearing impairment. *Neurology* **95**(16), e2225–e2234. PMID: 32878991; doi: 10.1212/WNL.0000000000010709.
21. Liu Y., Fang S., Liu L.-M., Zhu Y., Li C.-R., Chen K., & Zhao H.-B. (2020). Hearing loss is an early biomarker in APP/PS1 Alzheimer's disease mice. *Neurosci. Lett.* **717**, 134705. PMID: 31870800; doi: 10.1016/j.neulet.2019.134705.
22. O'Leary T.P., Shin S., Fertan E., Dingle R.N., Almuklass A., Gunn R.K., … Brown R.E. (2017). Reduced acoustic startle response and peripheral hearing loss in the 5xFAD mouse model of Alzheimer's disease. *Genes. Brain. Behav.* **16**(5), 554–563. PMID: 28133939; doi: 10.1111/gbb.12370.
23. Oddo S., Caccamo A., Shepherd J.D., Murphy M.P., Golde T.E., Kayed R., … LaFerla F.M. (2003). Triple-transgenic model of Alzheimer's disease with plaques and tangles: Intracellular Abeta and synaptic dysfunction. *Neuron* **39**(3), 409–421. PMID: 12895417; doi: 10.1016/S0896-6273(03)00434-3.
24. Wang S.-E., & Wu C.-H. (2021). Tau phosphorylation and cochlear apoptosis cause hearing loss in 3×Tg-AD mouse model of Alzheimer's disease. *Chin. J. Physiol.* **64**(2), 61–71. PMID: 33938816; doi: 10.4103/CJP.CJP_79_20.
25. Géléoc G.S.G., & Holt J.R. (2003). Developmental acquisition of sensory transduction in hair cells of the mouse inner ear. *Nat. Neurosci.* **6**(10), 1019–1020. PMID: 12973354; doi: 10.1038/nn1120.
26. Wagner E.L., & Shin J.-B. (2019). Mechanisms of hair cell damage and repair. *Trends Neurosci.* **42**(6), 414–424. PMID: 30992136; doi: 10.1016/j.tins.2019.03.006.
27. Bohne B.A., & Harding G.W. (2000). Degeneration in the cochlea after noise damage: Primary versus secondary events. *Am. J. Otol.* **21**(4), 505–509. PMID: 10912695.
28. Géléoc G.S.G., & Holt J.R. (2014). Sound strategies for hearing restoration. *Science* **344**(6184), 1241062. PMID: 24812404; doi: 10.1126/science.1241062.
29. Wong A.C.Y., & Ryan A.F. (2015). Mechanisms of sensorineural cell damage, death and survival in the cochlea. *Front. Aging Neurosci.* **7**, 58. PMID: 25954196; doi: 10.3389/fnagi.2015.00058.
30. Yu X., Liu W., Fan Z., Qian F., Zhang D., Han Y., … Wang H. (2017). c-Myb knockdown increases the neomycin-induced damage to hair-cell-like HEI-OC1 cells in vitro. *Sci. Rep.* **7**, 41094. PMID: 28112219; doi: 10.1038/srep41094.
31. Liang W., Zhao C., Chen Z., Yang Z., Liu K., & Gong S. (2021). Sirtuin-3 protects cochlear hair cells against noise-induced damage via the superoxide dismutase 2/reactive oxygen species signaling pathway. *Front. Cell Dev. Biol.* **9**, 766512. PMID: 34869361; doi: 10.3389/fcell.2021.766512.
32. Li A., You D., Li W., Cui Y., He Y., Li W., … Li H. (2018). Novel compounds protect auditory hair cells against gentamycin-induced apoptosis by maintaining the expression level of H3K4me2. *Drug Deliv.* **25**(1), 1033–1043. PMID: 30799660; doi: 10.1080/10717544.2018.1461277.
33. Sykora P., Misiak M., Wang Y., Ghosh S., Leandro G.S., Liu D., … Bohr V.A. (2015). DNA polymerase β deficiency leads to neurodegeneration and exacerbates Alzheimer disease phenotypes. *Nucleic Acids Res.* **43**(2), 943–959. PMID: 25552414; doi: 10.1093/nar/gku1356.
34. Hou Y., Lautrup S., Cordonnier S., Wang Y., Croteau D.L., Zavala E., … Bohr V.A. (2018). NAD+ supplementation normalizes key Alzheimer's features and DNA damage responses in a new AD mouse model with introduced DNA repair deficiency. *Proc. Natl. Acad. Sci. U. S. A.* **115**(8), E1876–E1885. PMID: 29432159; doi: 10.1073/pnas.1718819115.
35. Misiak M., Vergara Greeno R., Baptiste B.A., Sykora P., Liu D., Cordonnier S., … Bohr V.A. (2017). DNA polymerase β decrement triggers death of olfactory bulb cells and impairs olfaction in a mouse model of Alzheimer's disease. *Aging Cell* **16**(1), 162–172. PMID: 27686631; doi: 10.1111/acel.12541.
36. Lin X., Kapoor A., Gu Y., Chow M.J., Peng J., Zhao K., & Tang D. (2020). Contributions of DNA damage to alzheimer's disease. *Int. J. Mol. Sci.* **21**(5). PMID: 32121304; doi: 10.3390/ijms21051666.
37. Weissman L., Jo D.-G., Sørensen M.M., de Souza-Pinto N.C., Markesbery W.R., Mattson M.P., & Bohr V.A. (2007). Defective DNA base excision repair in brain from individuals with Alzheimer's disease and amnestic mild cognitive impairment. *Nucleic Acids Res.* **35**(16), 5545–5555. PMID: 17704129; doi: 10.1093/nar/gkm605.
38. Gabbita S.P., Lovell M.A., & Markesbery W.R. (1998). Increased nuclear DNA oxidation in the brain in Alzheimer's disease. *J. Neurochem.* **71**(5), 2034–2040. PMID: 9798928; doi: 10.1046/j.1471-4159.1998.71052034.x.
39. Lyras L., Cairns N.J., Jenner A., Jenner P., & Halliwell B. (1997). An assessment of oxidative damage to proteins, lipids, and DNA in brain from patients with Alzheimer's disease. *J. Neurochem.* **68**(5), 2061–2069. PMID: 9109533; doi: 10.1046/j.1471-4159.1997.68052061.x.
40. Wang J., Markesbery W.R., & Lovell M.A. (2006). Increased oxidative damage in nuclear and mitochondrial DNA in mild cognitive impairment. *J. Neurochem.* **96**(3), 825–832. PMID: 16405502; doi: 10.1111/j.1471-4159.2005.03615.x.
41. Lovell M.A., & Markesbery W.R. (2007). Oxidative DNA damage in mild cognitive impairment and late-stage Alzheimer's disease. *Nucleic Acids Res.* **35**(22), 7497–7504. PMID: 17947327; doi: 10.1093/nar/gkm821.
42. Bradley-Whitman M.A., Timmons M.D., Beckett T.L., Murphy M.P., Lynn B.C., & Lovell M.A. (2014). Nucleic acid oxidation: an early feature of Alzheimer's disease. *J. Neurochem.* **128**(2), 294–304. PMID: 24032632; doi: 10.1111/jnc.12444.
43. Myung N.-H., Zhu X., Kruman I.I., Castellani R.J., Petersen R.B., Siedlak S.L., … Lee H. (2008). Evidence of DNA damage in Alzheimer disease: phosphorylation of histone H2AX in astrocytes. *Age (Dordr.)* **30**(4), 209–215. PMID: 19424844; doi: 10.1007/s11357-008-9050-7.
44. Çağlar Ö, Çobanoğlu H., Uslu A., & Çayır A. (2021). Evaluation of DNA damages in congenital hearing loss patients. *Mutat. Res.* **822**, 111744. PMID: 33934048; doi: 10.1016/j.mrfmmm.2021.111744.
45. Okur M.N., Mao B., Kimura R., Haraczy S., Fitzgerald T., Edwards-Hollingsworth K., … Bohr V.A. (2020). Short-term NAD+ supplementation prevents hearing loss in mouse models of Cockayne syndrome. *NPJ Aging Mech. Dis.* **6**(1), 1. PMID: 31934345; doi: 10.1038/s41514-019-0040-z.
46. Jewett D.L., & Williston J.S. (1971). Auditory-evoked far fields averaged from the scalp of humans. *Brain* **94**(4), 681–696. PMID: 5132966; doi: 10.1093/brain/94.4.681.
47. Wilkinson A.R., & Jiang Z.D. (2006). Brainstem auditory evoked response in neonatal neurology. *Semin. Fetal Neonatal Med.* **11**(6), 444–451. PMID: 17015048; doi: 10.1016/j.siny.2006.07.005.
48. Källstrand J., Lewander T., Baghdassarian E., & Nielzén S. (2014). A new method for analyzing auditory brain-stem response waveforms using a moving-minimum subtraction procedure of digitized analog recordings. *Neuropsychiatr. Dis. Treat.* **10**, 1011–1016. PMID: 24944514; doi: 10.2147/NDT.S59178.

49. Urata S., & Okabe S. (2023). Three-dimensional mouse cochlea imaging based on the modified Sca/eS using confocal microscopy. *Anat. Sci. Int.* PMID: 36773194; doi: 10.1007/s12565-023-00703-z.

50. Hofstetter K.M., & Ehret G. (1992). The auditory cortex of the mouse: connections of the ultrasonic field. *J. Comp. Neurol.* **323**(3), 370–386. PMID: 1460109; doi: 10.1002/cne.903230306.

51. Rudolph J., Mahadevan J., Dyer P., & Luger K. (2018). Poly(ADP-ribose) polymerase 1 searches DNA via a "monkey bar" mechanism. *eLife* **7**. PMID: 30088474; doi: 10.7554/eLife.37818.

52. Herceg Z., & Wang Z.Q. (2001). Functions of poly(ADP-ribose) polymerase (PARP) in DNA repair, genomic integrity and cell death. *Mutat. Res.* **477** (1–2), 97–110. PMID: 11376691; doi: 10.1016/S0027-5107(01)00111-7.

53. Covarrubias A.J., Perrone R., Grozio A., & Verdin E. (2021). NAD+ metabolism and its roles in cellular processes during ageing. *Nat. Rev. Mol. Cell Biol.* **22**(2), 119–141. PMID: 33353981; doi: 10.1038/s41580-020-00313-x.

54. García-Añoveros J., Clancy J.C., Foo C.Z., García-Gómez I., Zhou Y., Homma K., … Duggan A. (2022). Tbx2 is a master regulator of inner versus outer hair cell differentiation. *Nature* **605**(7909), 298–303. PMID: 35508658; doi: 10.1038/s41586-022-04668-3.

55. Patel S., Shah L., Dang N., Tan X., Almudevar A., & White P.M. (2020). SIRT3 promotes auditory function in young adult FVB/nJ mice but is dispensable for hearing recovery after noise exposure. *PLoS ONE* **15**(7), e0235491. PMID: 32658908; doi: 10.1371/journal.pone.0235491.

56. Kong X., Wang R., Xue Y., Liu X., Zhang H., Chen Y., … Chang Y. (2010). Sirtuin 3, a new target of PGC-1alpha, plays an important role in the suppression of ROS and mitochondrial biogenesis. *PLoS ONE* **5**(7), e11707. PMID: 20661474; doi: 10.1371/journal.pone.0011707.

57. Bause A.S., & Haigis M.C. (2013). SIRT3 regulation of mitochondrial oxidative stress. *Exp. Gerontol.* **48**(7), 634–639. PMID: 22964489; doi: 10.1016/j.exger.2012.08.007.

58. Park J.-H., Burgess J.D., Faroqi A.H., DeMeo N.N., Fiesel F.C., Springer W., … McLean P.J. (2020). Alpha-synuclein-induced mitochondrial dysfunction is mediated via a sirtuin 3-dependent pathway. *Mol. Neurodegener.* **15**(1), 5. PMID: 31931835; doi: 10.1186/s13024-019-0349-x.

59. Sharma N., Pasala M.S., & Prakash A. (2019). Mitochondrial DNA: Epigenetics and environment. *Environ. Mol. Mutagen.* **60**(8), 668–682. PMID: 31335990; doi: 10.1002/em.22319.

60. Hoffman H.J., Dobie R.A., Losonczy K.G., Themann C.L., & Flamme G.A. (2017). Declining prevalence of hearing loss in US adults aged 20 to 69 years. *JAMA Otolaryngol. Head Neck Surg.* **143**(3), 274–285. PMID: 27978564; doi: 10.1001/jamaoto.2016.3527.

61. Bowman D.M., Brown D.K., & Kimberley B.P. (2000). An examination of gender differences in DPOAE phase delay measurements in normal-hearing human adults. *Hear. Res.* **142**(1–2), 1–11. PMID: 10748323; doi: 10.1016/S0378-5955(99)00212-9.

62. Mielke M.M. (2018). Sex and gender differences in alzheimer's disease dementia. *Psychiatr. Times* **35**(11), 14–17. PMID: 30820070.

63. Lien K.-H., & Yang C.-H. (2021). Sex differences in the triad of acquired sensorineural hearing loss. *Int. J. Mol. Sci.* **22**(15). PMID: 34360877; doi: 10.3390/ijms22158111.

64. Stenberg A.E., Wang H., Sahlin L., & Hultcrantz M. (1999). Mapping of estrogen receptors alpha and beta in the inner ear of mouse and rat. *Hear. Res.* **136**(1–2), 29–34. PMID: 10511621; doi: 10.1016/S0378-5955(99)00098-2.

65. Demarest T.G., Varma V.R., Estrada D., Babbar M., Basu S., Mahajan U.V., … Bohr V.A. (2020). Biological sex and DNA repair deficiency drive Alzheimer's disease via systemic metabolic remodeling and brain mitochondrial dysfunction. *Acta Neuropathol.* **140**(1), 25–47. PMID: 32333098; doi: 10.1007/s00401-020-02152-8.

66. Castro A.C., & Monteiro P. (2022). Auditory dysfunction in animal models of autism spectrum disorder. *Front. Mol. Neurosci.* **15**, 845155. PMID: 35493332; doi: 10.3389/fnmol.2022.845155.

67. Di Bonito M., & Studer M. (2017). Cellular and molecular underpinnings of neuronal assembly in the central auditory system during mouse development. *Front. Neural. Circuits* **11**, 18. PMID: 28469562; doi: 10.3389/fncir.2017.00018.

68. Malmierca M.S. (2003). The structure and physiology of the rat auditory system: An overview. *Int. Rev. Neurobiol.* **56**, 147–211. PMID: 14696313; doi: 10.1016/s0074-7742(03)56005-6.

69. Hinojosa R., Nelson E.G., Lerner S.A., Redleaf M.I., & Schramm D.R. (2001). Aminoglycoside ototoxicity: A human temporal bone study. *Laryngoscope* **111**(10), 1797–1805. PMID: 11801948; doi: 10.1097/00005537-200110000-00025.

70. Scheffer D.I., Shen J., Corey D.P., & Chen Z.-Y. (2015). Gene expression by mouse inner ear hair cells during development. *J. Neurosci.* **35**(16), 6366–6380. PMID: 25904789; doi: 10.1523/JNEUROSCI.5126-14.2015.

71. Rot I., Baguma-Nibasheka M., Costain W.J., Hong P., Tafra R., Mardesic-Brakus S., … Kablar B. (2017). Role of skeletal muscle in ear development. *Histol. Histopathol.* **32**(10), 987–1000. PMID: 28271491; doi: 10.14670/HH-11-886.

72. Villavisanis D.F., Berson E.R., Lauer A.M., Cosetti M.K., & Schrode K.M. (2020). Sex-based differences in hearing loss: Perspectives from non-clinical research to clinical outcomess. *Otol. Neurotol.* **41**(3), 290–298. PMID: 31789968; doi: 10.1097/MAO.0000000000002507.

73. Li M., Gao X., Wang H., Zhang M., Li X., Wang S., … Su G. (2021). Phosphoglycerate mutase 2 is elevated in serum of patients with heart failure and correlates with the disease severity and patient's prognosis. *Open Med. (Wars)* **16**(1), 1134–1142. PMID: 34435138; doi: 10.1515/med-2021-0324.

74. Qiu H., Zhao S., Xu X., Yerle M., & Liu B. (2008). Assignment and expression patterns of porcine muscle-specific isoform of phosphoglycerate mutase gene. *J. Genet. Genomics.* **35**(5), 257–260. PMID: 18499067; doi: 10.1016/S1673-8527(08)60036-3.

75. Zhang Y., Beketaev I., Ma Y., & Wang J. (2022). Sumoylation-deficient phosphoglycerate mutase 2 impairs myogenic differentiation. *Front. Cell Dev. Biol.* **10**, 1052363. PMID: 36589741; doi: 10.3389/fcell.2022.1052363.

76. Hamezah H.S., Durani L.W., Yanagisawa D., Ibrahim N.F., Aizat W.M., Makpol S., … Tooyama I. (2019). Modulation of proteome profile in AβPP/PS1 mice hippocampus, medial prefrontal cortex, and striatum by palm oil derived tocotrienol-rich fraction. *J. Alzheimers Dis.* **72**(1), 229–246. PMID: 31594216; doi: 10.3233/JAD-181171.

77. Edmonds J.L., Kirse D.J., Kearns D., Deutsch R., Spruijt L., & Naviaux R.K. (2002). The otolaryngological manifestations of mitochondrial disease and the risk of neurodegeneration with infection. *Arch. Otolaryngol. Head Neck Surg.* **128**(4), 355–362. PMID: 11926907; doi: 10.1001/archotol.128.4.355.

78. Scarpelli M., Zappini F., Filosto M., Russignan A., Tonin P., & Tomelleri G. (2012). Mitochondrial sensorineural hearing loss: A retrospective study and a description of cochlear implantation in a MELAS patient. *Genet. Res. Int.* **2012**, 287432. PMID: 22567382; doi: 10.1155/2012/287432.

79. Yang W., Nagasawa K., Münch C., Xu Y., Satterstrom K., Jeong S., … Haigis M.C. (2016). Mitochondrial sirtuin network reveals dynamic SIRT3-dependent deacetylation in response to membrane depolarization. *Cell* **167**(4), 985–1000.e21. PMID: 27881304; doi: 10.1016/j.cell.2016.10.016.

80. Brown K.D., Maqsood S., Huang J.-Y., Pan Y., Harkcom W., Li W., … Jaffrey S.R. (2014). Activation of SIRT3 by the NAD+ precursor nicotinamide riboside protects from noise-induced hearing loss. *Cell Metab.* **20**(6), 1059–1068. PMID: 25470550; doi: 10.1016/j.cmet.2014.11.003.

81. Someya S., Yu W., Hallows W.C., Xu J., Vann J.M., Leeuwenburgh C., … Prolla T.A. (2010). Sirt3 mediates reduction of oxidative damage and prevention of age-related hearing loss under caloric restriction. *Cell* **143** (5), 802–812. PMID: 21094524; doi: 10.1016/j.cell.2010.10.002.

82. Raimundo N., Song L., Shutt T.E., McKay S.E., Cotney J., Guan M.-X., … Shadel G.S. (2012). Mitochondrial stress engages E2F1 apoptotic signaling to cause deafness. *Cell* **148**(4), 716–726. PMID: 22341444; doi: 10.1016/j.cell.2011.12.027.

83. Peng Z., Zhao C., Yang Z., Gong S., & Du Z. (2023). D-galactose-induced mitochondrial oxidative damage and apoptosis in the cochlear stria vascularis of mice. *BMC Mol. and Cell Biol.* **24**(1), 27. PMID: 37605129; doi: 10.1186/s12860-023-00480-7.